



1 **Development of an instrument for direct ozone production rate measurements: Measurement**
2 **reliability and current limitations**

3 Sofia Sklaveniti^{1,2}, Nadine Locoge¹, Philip S. Stevens^{2,3}, Ezra Wood^{4,5}, Shuvashish Kundu⁴, Sebastien
4 Dusanter¹

5 [1] IMT Lille Douai, Univ. Lille, SAGE - Département Sciences de l'Atmosphère et Génie de
6 l'Environnement, 59000 Lille, France

7 [2] School of Public and Environmental Affairs, Indiana University, Bloomington, IN 47405, USA

8 [3] Department of Chemistry, Indiana University, Bloomington, IN, USA

9 [4] Department of Chemistry, University of Massachusetts, Amherst, MA USA

10 [5] Department of Chemistry, Drexel University, Philadelphia, PA, USA

11 **Abstract**

12 Ground level ozone (O₃) is an important pollutant that affects both global climate change and regional
13 air quality, with the latter linked to detrimental effects on both human health and ecosystems. Ozone
14 is not directly emitted in the atmosphere but is formed from chemical reactions involving volatile
15 organic compounds (VOCs), nitrogen oxides (NO_x = NO+NO₂) and sunlight. The photochemical
16 nature of ozone makes the implementation of reduction strategies challenging and a good
17 understanding of its formation chemistry is fundamental in order to develop efficient strategies of
18 ozone reduction from mitigation measures of primary VOCs and NO_x emissions.

19 An instrument for direct measurements of ozone production rates (OPR) was developed and deployed
20 in the field as part of the IRRONIC (Indiana Radical, Reactivity and Ozone production
21 InterComparison) field campaign. The OPR instrument is based on the principle of the previously
22 published MOPS instrument (Measurement of Ozone Production Sensor) but using a different
23 sampling design made of quartz flow tubes and a different O_x (O₃ and NO₂) conversion/detection
24 scheme composed of an O₃-to-NO₂ conversion unit and a Cavity Attenuated Phase Shift (CAPS) NO₂
25 monitor. Tests performed in the laboratory and in the field, together with model simulations of the



1 radical chemistry occurring inside the flow tubes, were used to assess (i) the reliability of the
2 measurement principle and (ii) potential biases associated to OPR measurements.

3 This publication reports the first field measurements made using this instrument to illustrate its
4 performance. The results showed that a photo-enhanced loss of ozone inside the sampling flow tubes
5 disturb the measurements. This issue needs to be solved to be able to perform accurate ambient
6 measurements of ozone production rates with the instrument described in this study. However, an
7 attempt was made to investigate the OPR sensitivity to NO_x by adding NO inside the instrument. This
8 type of investigations does not require measuring ambient OPR but only probing the change in ozone
9 production when NO is added. During IRRONIC, changes in ozone production rates ranging from the
10 limit of detection (3σ) of 6.2 ppbv h^{-1} up to 20 ppbv h^{-1} were observed when 6 ppbv of NO was added
11 into the flow tubes.

12 **1 Introduction**

13 Ground-level ozone (O_3) is a primary constituent of photochemical smog that irritates the respiratory
14 system (WHO, 2013) and damages vegetation (Ashmore, 2005). In addition, ozone is a greenhouse
15 gas and an important precursor of the hydroxyl radical (OH), a key species controlling the
16 atmospheric oxidative capacity (Monks, 2005; Rohrer et al., 2014; Prinn, 2003). Ozone is a
17 photochemical pollutant formed during daytime and has an average lifetime estimated at 22 ± 2 days
18 (Stevenson et al., 2006), which is long enough to transport it from polluted regions to remote areas
19 and between continents. The local production of ozone on top of the amount advected from elsewhere
20 can lead to exceedances of air quality standards in urbanized areas, making ozone pollution an issue
21 of global concern (Akimoto, 2003).

22 In the troposphere, ozone can be rapidly converted to nitrogen dioxide (NO_2) through reaction with
23 nitric oxide (NO), and back to O_3 through NO_2 photolysis. This chemistry does not produce new
24 ozone and is known as the O_3 - NO_x PhotoStationary State (PSS), with NO_x being the sum of NO and
25 NO_2 . The production of new ozone is driven by the oxidation of Volatile Organic Compounds
26 (VOCs), which leads to the production of hydroperoxy (HO_2) and organic peroxy (RO_2) radicals. The



1 current understanding of tropospheric ozone chemistry indicates that new ozone is formed via
 2 reactions of these peroxy radicals with NO, which results in the conversion of NO to NO₂ without
 3 consumption of ozone (Monks, 2005; Seinfeld and Pandis, 2006).

4 When ozone is produced, reactions of peroxy radicals with NO also lead to the formation of OH,
 5 which can then oxidize other molecules of VOCs to produce more peroxy radicals, and as a
 6 consequence, more ozone. The propagation chemistry between RO_x (OH, HO₂ and RO₂) radicals,
 7 which fuels ozone production, is terminated either by NO_x-RO_x reactions or by cross reactions of RO_x
 8 radicals in NO_x-rich and NO_x-poor environments, respectively. These two types of termination
 9 reactions lead to different regimes of ozone production referred as NO_x-limited or NO_x-saturated
 10 when the rate of ozone production increases or decreases with NO_x, respectively. The turnover point
 11 between the two regimes depends on NO_x concentrations, VOC reactivity, and radical production
 12 rates (Kleinman, 2005). Since different air quality regulations have to be implemented for the two
 13 different regimes, i.e either NO_x or VOC emission regulations, the understanding of the complex and
 14 non-linear radical chemistry is key for the design of efficient emission control strategies.

15 The instantaneous ozone production rate, $p(O_3)$, can be calculated from Equation (1) as the rate of
 16 reactions between peroxy radicals and NO. The instantaneous ozone loss rate, $l(O_3)$, can be calculated
 17 using Equation (2), based on reaction rates for ozone photolysis, reactions of O₃ with HO_x and
 18 alkenes, and the reaction of OH with NO₂, since NO₂ is a reservoir molecule for O₃. The net ozone
 19 production rate, $P(O_3)$, is then computed as the difference between instantaneous production and loss
 20 rates (Eq. (3)):

$$21 \quad p(O_3) = k_{HO_2+NO}[HO_2][NO] + \sum_i (k_{RO_{2,i}+NO}[RO_{2,i}][NO]) \quad (1)$$

$$22 \quad l(O_3) =$$

$$23 \quad k_{O(^1D)+H_2O}[O(^1D)][H_2O] + k_{OH+O_3}[OH][O_3] + k_{HO_2+O_3}[HO_2][O_3] +$$

$$24 \quad \sum_i k_{O_3+Alkene_i}[O_3][Alkene_i] + k_{OH+NO_2}[OH][NO_2] \quad (2)$$

$$25 \quad P(O_3) = p(O_3) - l(O_3) \quad (3)$$



1 Here k_{X+Y} is the bimolecular reaction rate constant for the two reagents X and Y. Therefore, the
2 calculation of ozone production rates requires peroxy radical concentrations, either from ambient
3 measurements (Green et al., 2006;Liu and Zhang, 2014;Fuchs et al., 2008;Dusanter et al.,
4 2009a;Griffith et al., 2016) or box model outputs (Goliff et al., 2013;Stockwell et al., 2011;Saunders
5 et al., 2003).

6 In most urban and suburban environments, where concentrations of NO_x are significant (10-80 ppbv),
7 ozone production rates can reach a few tens of ppbv h^{-1} (Mao et al., 2010). In highly polluted
8 environments, such as Mexico City or Houston, TX, $\text{P}(\text{O}_3)$ can even exceed 100 ppbv h^{-1} (Shirley et
9 al., 2006;Chen et al., 2010). Ozone production rates lower than 10 ppbv h^{-1} have also been observed in
10 urban atmospheres such as Phoenix, AZ (Kleinman et al., 2002), likely due to lower initiation rates of
11 radicals. Ozone production is usually low in more remote areas or forested environments that are not
12 impacted by anthropogenic activities (less than $2\text{-}3 \text{ ppbv h}^{-1}$), due to the low NO_x concentrations
13 (Geng et al., 2011). However, if NO_x emission sources are located downwind of a forested area,
14 highly reactive biogenic VOCs (e.g. isoprene) can lead to an enhancement of ozone production (Geng
15 et al., 2011;Thornton et al., 2002).

16 Some studies performed in urban and suburban areas, whose objectives were to test our understanding
17 of the radical chemistry by contrasting measurements and model simulations of HO_x concentrations,
18 showed that models tend to underestimate HO_2 for NO mixing ratios higher than a few ppbv (Ren et
19 al., 2013;Chen et al., 2010;Dusanter et al., 2009b;Kanaya et al., 2007;Ren et al., 2003). In contrast,
20 models tend to overestimate HO_2 in forested areas and regions characterized by large concentrations
21 of biogenic VOCs (Griffith et al., 2013;Mao et al., 2012;Pugh et al., 2010). Disagreements are also
22 present in the modeling of OH, with the models underestimating the measurements at forested
23 environments (Lelieveld et al., 2008;Tan et al., 2001;Whalley et al., 2011;Hofzumahaus et al.,
24 2009;Lu et al., 2013;Pugh et al., 2010), while the agreement may be better when colder temperatures
25 lead to lower concentrations of isoprene and other VOCs (Griffith et al., 2013). The discrepancies
26 between models and measurements question our ability to successfully measure radical species or
27 indicate that there are still unknowns in our understanding of the radical and ozone production



1 chemistry, which in turn could lead to erroneous $P(O_3)$ calculations by atmospheric models. These
2 models are widely used for the design of air quality regulations (Rao et al., 2010; Fu et al., 2006)
3 based on emission control strategies. It is therefore essential to ensure that chemical mechanisms used
4 in atmospheric models are accurate enough to simulate the oxidative capacity of the atmosphere and
5 to predict both absolute rates of ozone production and the turnover point between the two ozone
6 production regimes.

7 In order to address these issues, an instrument for direct ozone production measurements (MOPS) was
8 developed by Cazorla and Brune (2010). The principle of MOPS is based on differential ozone
9 measurements between two sampling chambers made of FEP, one exposed to sunlight (referred as
10 sampling chamber) to get an ozone production rate inside the chamber that mimics atmospheric $P(O_3)$
11 and the other one covered with a UV filter (reference chamber) to suppress the radical chemistry, and
12 as a consequence, ozone production. The difference in ozone between the two chambers divided by
13 the exposure time yields the ozone production rate. However, NO_2 can act as a reservoir molecule for
14 O_3 due to the rapid interconversion between these two species and NO_2 has to be converted into O_3
15 before measuring ozone. The differential O_x ($O_x=O_3+NO_2$) measurements yields $P(O_x)$ values, which
16 represent $P(O_3)$ when NO_2 is efficiently photolyzed during daytime.

17 The first version of the MOPS instrument was tested on the campus of Pennsylvania State University
18 in the late summer of 2008. These tests demonstrated the feasibility of the MOPS technique, as the
19 instrument responded to the presence of solar radiation and ozone precursors and yielded rates of
20 ozone production that were within a range of reasonable values (up to 10 ppbv h^{-1}) for this area. This
21 instrument was then deployed during the Study of Houston Atmospheric Radical Precursors (SHARP,
22 2009) (Cazorla et al., 2012). The measurements were compared to ozone production rates calculated
23 using measurements of HO_2 and NO (referred as calculated $P(O_3)$) as well as modeled radical
24 concentrations from a box model (referred as modeled $P(O_3)$). Measured and calculated $P(O_3)$ had
25 similar peak values but the calculated $P(O_3)$ tended to peak earlier in the morning when NO values
26 were higher. Measured and modeled $P(O_3)$ had a similar diurnal profile, but the modeled $P(O_3)$ was
27 only half the measured $P(O_3)$. The MOPS deployment during the SHARP field campaign showed the



1 potential of this instrument for contributing to the understanding of the ozone-producing chemistry,
2 but was limited by measurement uncertainties due to potential wall effects. The heterogeneous loss of
3 NO₂ under humid conditions (RH > 50%) was reported as a main issue for this technique.

4 Recently, an improved version of the MOPS instrument was deployed during the NASA's
5 DISCOVER-AQ field campaign in 2013, in Houston, Texas (Baier et al., 2015). Wall effects were
6 reduced by improving the design of the sampling chambers and the airflow characteristics. The
7 measurements made over one month were consistent with ambient ozone observations and model-
8 derived P(O₃) values from previous field campaigns in Houston. The authors, however, highlighted a
9 possible bias due to surface HONO production followed by its photolysis in the sampling chamber, as
10 well as unresolved ozone analyzer issues. HONO concentrations in the sampling chambers were
11 reported as two to five times higher than ambient values, which could cause a bias up to 5-10 ppbv h⁻¹
12 on the P(O₃) measurements.

13 In this publication, we present the development and the characterization of an Ozone Production Rates
14 (OPR) instrument. The OPR instrument is based on the principle of the MOPS, using different
15 sampling and detection schemes. This publication describes this new instrument and its
16 characterization in the laboratory. An emphasis is given to the modeling of the radical chemistry
17 inside the sampling chambers to assess potential biases on P(O₃) measurements associated to
18 instrumental characteristics and operating conditions. The publication also reports preliminary field
19 results from the Indiana Radical, Reactivity and Ozone Production Intercomparison (IRRONIC)
20 campaign, which highlight the current limitations of this instrument.

21 **2 Experimental section**

22 **2.1 Description of the OPR instrument**

23 The principle of the OPR is based on differential O_x measurements between an “ambient” flow tube,
24 exposed to sunlight to mimic ambient photochemistry, and a “reference” flow tube, covered with an
25 Ultem® film (polyetherimide, 0.25 mm thick, CS Hyde Co, USA) to block wavelengths lower than
26 400 nm, which in turn should suppress ozone production. As mentioned above for the MOPS



1 instrument, the fast partitioning between O_3 and NO_2 requires measuring O_x instead of O_3 , assuming
2 that $P(O_3)$ is equal to $P(O_x)$ when NO_2 is efficiently photolyzed during daytime. $P(O_x)$ is calculated
3 from the difference in O_x between the two flow tubes, ΔO_x , divided by the mean residence time (τ) of
4 air inside the tubes:

$$5 \quad P(O_x) = \frac{\Delta O_x}{\tau} = \frac{O_{xamb} - O_{xref}}{\tau} \quad (4)$$

6 A detailed schematic of the OPR instrument is shown in Figure 1. The two flow tubes exhibit the
7 same geometry and are made of quartz (14 cm-ID and 70 cm long). Each flow tube is connected to the
8 inlet and outlet flanges that are made of anodized aluminum and PTFE. Since a major issue previously
9 identified for the MOPS instrument was wall effects causing NO_2 losses (Cazorla and Brune, 2010),
10 the inner geometry of the flanges was designed based on fluid dynamics simulations using STAR
11 CCM+ V.8 (CD-adapco). The geometry was optimized to minimize radial mixing and recirculation
12 eddies that could increase wall effects. The design of the flanges can be found in the supplementary
13 material (Fig. S1).

14 Each flange consists of two parts. For both the inlet and outlet, a conical PTFE piece is screwed inside
15 an external aluminum flange. Four holes are drilled symmetrically around the aluminum flanges to
16 inject zero air around the PTFE inlet and to extract air around the PTFE outlet. The lengths of the inlet
17 and outlet flanges are 25 and 14 cm, respectively. The PTFE inlet has an external diameter of 2.54 cm
18 which increases to 7 cm over a length of 20 cm. The PTFE outlet starts from a diameter of 3 cm
19 which decreases to 1.27 cm over 10 cm. The aluminum flanges exhibit a curved conical inner surface
20 around the PTFE parts.

21 Ambient air is sampled through a common inlet (PFA, 1.27 cm-OD) at a flow rate of 4 L min^{-1} and is
22 transferred into both flow tubes through the internal PTFE inlets (2 L min^{-1}), while additional zero air
23 (250 mL min^{-1}) is injected at the outer periphery of these inlets inside the flanges. This flow of zero
24 air helps keeping the ambient air flow forward, minimizing recirculation eddies, and therefore
25 reducing wall effects. The dilution of the sampled air is approximately 10%. At the outlet, air is
26 sampled only from the center of the flow tube, through the PTFE outlet (750 mL min^{-1}), while the rest



1 is extracted by an external pump (1.5 L min^{-1}). Both the injection and extraction of air are regulated
2 by mass flow controllers (MFC in Fig. 1).

3 The Ultem filter is placed on a rectangular aluminum frame outside of the reference flow tube, which
4 enables to flow ambient air between the filter and the flow tube using fans. This setup allows the two
5 flow tubes to be kept at the same temperature by extracting the heat released by the filter. For the
6 same reason, a frame covered by a FEP film ($.002''$ thick, DuPont Teflon® FEP), transparent to the
7 solar radiation, is used for the ambient flow tube to reduce heat dissipation by the wind.

8 The air exiting the two flow tubes is mixed with 10 SCCM of NO (50 ppmv, Indiana Oxygen, USA),
9 leading to a NO mixing ratio of 650 ppbv in the conversion unit. The mixing of the gases takes place
10 in two identical pyrex chambers, providing a reaction time of approximately 22 sec at 20°C , which is
11 long enough to quantitatively titrate O_3 into NO_2 . Both the relative humidity and temperature are
12 monitored in the air flow extracted from the flow tubes and at the O_3 -to- NO_2 conversion unit.

13 Downstream the conversion unit, O_x ($\text{O}_3 + \text{NO}_2$) is measured by an Aerodyne Cavity Attenuated
14 Phase Shift Spectroscopy (CAPS) NO_2 monitor (Kebabian et al., 2005;Kebabian et al., 2008). The
15 detection limit (3σ) for a 1-s integration time is 300 pptv. Since the CAPS is a single-cell monitor, the
16 measurements from the ambient and reference flow tubes are taken sequentially, using two solenoid
17 valves (SV1 and SV2 in Fig. 1). When air from the ambient (or reference) flow tube is sampled by the
18 CAPS monitor (750 ml min^{-1}), the same flow rate of air is extracted from the other flow tube by a
19 mass flow controller connected to a pump. The valves switch every 1 min, alternating the flows that
20 are sampled by the CAPS monitor and the pump. ΔO_x is calculated as the difference between an
21 ambient flow tube measurement and the average of 2 surrounding reference measurements, leading to
22 a $\text{P}(\text{O}_x)$ measurement every 2 min. The first 15 seconds of each 1-min measurement are discarded
23 since they describe a transient regime between ambient and reference flow tube measurements. Ozone
24 production values are calculated from Eq. (4).

25 The measurement sequence is automated and controlled through a National Instruments LabView
26 2013 interface. Three USB data acquisition boards are used (NI-9264, NI-6008, NI-6009) to control



1 the two solenoid valves and the seven mass flow controllers, as well as to record signals from the
2 CAPS monitor and sensors setup for humidity and temperature measurements.

3 **2.2 Laboratory and field experiments conducted to characterize the OPR**

4 Experiments conducted to characterize the OPR instrument include measurements of the mean
5 residence time, O_x losses, and HONO production rates in the flow tubes and measurements of the O₃-
6 to-NO₂ conversion efficiency.

7 **The mean residence time** was quantified in each flow tube by injecting short pulses of toluene (10-s
8 in duration) at the inlet of the flow tubes. A PTR-ToFMS (Proton Transfer Reaction–Time of Flight
9 Mass Spectrometer, KORE Technology Inc.) was connected at the outlets to measure the time it takes
10 for a pulse introduced at the inlets to exit the flow tubes. The pulse experiment was repeated 5 times,
11 and the average was calculated as the mean residence time.

12 **O₃ and NO₂ losses** inside both flow tubes were measured in the laboratory and during the field
13 deployment described below by sampling mixtures of zero air and O₃ (or NO₂) at known mixing ratios
14 and by measuring NO₂ downstream the conversion unit (or directly at the exit of the flow tubes). A
15 relative loss was calculated from the difference in concentrations between the inlet and outlet and was
16 referenced to the inlet concentration. These tests were performed at relative humidity values ranging
17 from 0–65%.

18 **The release of HONO from the inner surface of the flow tubes** was quantified using a Chemical
19 Ionization Mass Spectrometer (CIMS, Georgia Tech). Mixtures of NO₂ and humid zero air were
20 introduced into the flow tubes, while HONO was measured both at the inlet and outlet. These
21 experiments were performed under dark conditions, as well as under various irradiated conditions
22 using artificial UV light provided by two types of fluorescent lamps: 4 lamps centered at 312 nm
23 (Vilber, T-15.M) and 4 lamps centered at 365 nm (Philips, T12).

24 Finally, the **O₃-to-NO₂ conversion efficiency** was measured by sampling zero air enriched with O₃
25 (3-170 ppbv) through the mixing chambers of the conversion unit, varying the flow of NO and
26 measuring NO₂ with the CAPS monitor. These tests were performed at various relative humidities



1 (25–60%). The conversion efficiency at a specific NO level was calculated from the ratio of NO₂
2 measured at this NO level to that measured when 700 ppbv of NO were added, assuming for the latter
3 that 100% of O₃ was converted. This assumption is verified from kinetic considerations
4 ($k_{\text{NO}+\text{O}_3}=1.80\times 10^{-14}$ cm³ molecule⁻¹ s⁻¹ and 23 s of residence time in the conversion unit) and from the
5 observation of a plateau for NO mixing ratios higher than 500 ppbv.

6 **2.3 Modeling experiments conducted to characterize the OPR**

7 As previously mentioned, the measurement principle of ozone production rates is based on the
8 assumption that (i) P(O_x) in the ambient flow tube is similar to P(O_x) in the atmosphere and (ii) there
9 is no significant production of ozone in the reference flow tube. Box model simulations were
10 performed to check whether this assumption is valid. In addition, simulations were also conducted to
11 investigate the impact on OPR measurements of (a) an O₃-to-NO₂ conversion efficiency lower than
12 100%, (b) NO₂ and O₃ losses and (c) HONO production inside the flow tubes, (d) a possible increase
13 of the temperature in the reference flow tube due to the UV filter, (e) the dilution of ambient air by
14 injecting zero air inside the flow tubes at the periphery of the inlets, and (f) reactions of OH with NO_x
15 species producing O_x.

16 **2.3.1 Selected data and chemical mechanism**

17 The simulations were performed using a box model based on the Regional Atmospheric Chemistry
18 Mechanism (RACM) (Stockwell et al., 1997). RACM is a gas-phase chemical mechanism developed
19 for the modeling of regional atmospheric chemistry and includes 17 stable inorganic species, 4
20 inorganic intermediates, 32 stable organic species and 24 organic intermediates for a total of 237
21 chemical reactions. Organic compounds are grouped together to form a manageable set of
22 compounds. Only 8 organic species are treated explicitly (methane, ethane, ethene, isoprene,
23 formaldehyde, glyoxal, methyl hydrogen peroxide and formic acid) and 24 are surrogates that are
24 grouped based on emission rates, chemical structure and reactivity with the OH radical.

25 Measurements from several field campaigns were used for this modeling exercise, including
26 measurements performed in (i) a megacity as part of the 2006 Mexico City Metropolitan Area
27 (MCMA-2006) (Dusanter et al., 2009b) and (ii) an urban area as part of the 2010 California Nexus



1 (CalNex) campaign (Griffith et al., 2016). Two days characterized by elevated and low O_x
2 concentrations were selected for each campaign and are presented in the supplementary material
3 (Table S1 and Fig. S2). For both campaigns, ozone was higher by approximately a factor 2 on high O_3
4 days (≈ 100 ppbv) compared to low O_3 days (≈ 50 ppbv). However, while both high and low ozone
5 levels were similar for the selected days of these campaigns, large differences were observed for NO_x
6 ($6\text{--}120$ ppbv) and OH reactivity ($8\text{--}86$ s⁻¹). Since OH reactivity and NO_x are main drivers of ozone
7 production, these modeling results are expected to provide a good assessment of potential biases
8 associated to $P(O_x)$ measurement for any urban environments.

9 **2.3.2 Modeling of ambient $P(O_x)$ values**

10 The model was constrained by 10-min (MCMA) or 15-min (CalNex) average measurements of
11 temperature, pressure, humidity, organic and inorganic species, and J-values, while the differential
12 equation system was integrated by the FACSIMILE solver (MCPA Software Ltd). In total, 24 J-
13 values were used to constrain the model, as derived in Dusanter et al. (2009b), together with 7
14 inorganic and 17 organic species or surrogates. Tables reporting the constrained species and J-values
15 can be found in the supplementary material (Tables S2 and S3). The integration time was set at 30h
16 with constrained species reinitialized every two seconds. Ambient ozone production values were then
17 calculated from Eq. (1)–(3) and are referred as $P(O_x)_{atm}$ in the following. In total, 18 surrogates of
18 RO_2 species were taken into account to calculate $p(O_3)$ from Eq. (1), while 10 unsaturated surrogates
19 were used to calculate $l(O_3)$ from Eq. (2) (Table S4).

20 **2.3.3 Modeling of $P(O_x)$ values in the ambient and reference flow tubes**

21 Modeling OPR measurements requires simulating the chemistry inside each flow tube. J-values used
22 to model the chemistry in the ambient flow tube were the same as for the ambient modeling since the
23 quartz material used to build the flow tubes is transparent to solar irradiation. For the reference flow
24 tube, J-values were scaled based on the absorption coefficient of the Ultem film (Philipp et al., 1989)
25 as discussed in the supplementary material (section S2.1).

26 The model was constrained by the same meteorological parameters and chemical species as for
27 $P(O_x)_{atm}$. In addition, modeled concentrations of VOC-oxidation products and peroxy radicals



1 inferred from the modeling of $P(O_x)_{atm}$ were also constrained in these simulations (Table S5),
 2 assuming that a significant fraction of the latter is not lost in the sampling line. The constrained
 3 concentrations were initialized once, at the entrance of the flow tubes, and the simulations were run
 4 for 10 minutes without reinitializing the constraints. The simulations were run separately for each
 5 flow tube and $P(O_x)$ was calculated every 15 s from Eq. (3). An integrated value of $P(O_x)$ was then
 6 computed for the flow tube residence time.

7 $P(O_x)_{atm}$ is compared to the integrated $P(O_x)$ value from the ambient flow tube (referred as
 8 $P(O_x)_{amb}$) to check whether ozone production in the ambient flow tube is similar to ambient ozone
 9 production. The integrated value of $P(O_x)$ in the reference flow tube (referred as $P(O_x)_{ref}$) is also
 10 scrutinized to check whether ozone production is negligible in this flow tube.

11 2.3.4 Modeling of OPR measurements

12 Since the OPR instrument measures O_x after conversion of O_3 into NO_2 , NO_2 concentrations at the
 13 exit of the conversion unit are calculated from the conversion efficiency C as shown in Eq. (5):

$$14 \quad [NO_2]_{conv} = [NO_2]_{\tau} + C [O_3]_{\tau} \quad :$$
 (5)

15 Here the concentrations reflect those observed at the exit of the conversion unit (subscript: *conv*) and
 16 at the exit of the flow tubes (subscript: τ). The concentrations at the exit of the flow tubes are the
 17 model outputs at the residence time τ . Based on Eq. (4), the ozone production rate measured by the
 18 OPR, $P(O_x)_{OPR}$, is then calculated from Eq. (6):

$$19 \quad P(O_x)_{OPR} = \frac{[NO_2]_{conv,amb} - [NO_2]_{conv,ref}}{\tau} = \frac{[NO_2]_{\tau,amb} - [NO_2]_{\tau,ref} + C([O_3]_{\tau,amb} - [O_3]_{\tau,ref})}{\tau}$$
 (6)

20 In this equation the subscripts *amb* and *ref* indicate the ambient and the reference flow tubes,
 21 respectively. A Bias in OPR measurements can be quantified by comparing $P(O_x)_{OPR}$ to $P(O_x)_{atm}$
 22 assuming a conversion efficiency of 100% for the conversion units.

23 2.3.5 Sensitivity tests

24 The simulation performed without O_x losses and HONO production in the flow tubes, no dilution, and
 25 no temperature differences between the tubes will be referred as base simulation in the following. All



1 simulations performed including sensitivity tests are compared to the results from the base simulation
2 to assess the impact of operating conditions on ozone production measurements.

3 To assess the impact of a conversion efficiency lower than 100%, $P(O_x)_{OPR}$ is calculated from Eq. (6)
4 by varying the conversion efficiency using the model outputs from the base simulation. $P(O_x)$ values
5 inferred when varying the conversion efficiency are compared to values calculated for a conversion
6 efficiency of 100%. To account for O_x losses, a similar sink of O_3 or NO_2 is introduced in the model
7 for each flow tube, with a first order loss rate ranging from 1.5×10^{-4} to $1.2 \times 10^{-3} \text{ s}^{-1}$. This range of loss
8 rates corresponds to a relative loss of 4–28%. The measured $P(O_x)_{OPR}$ is again calculated by Eq. (6)
9 assuming a conversion efficiency of 100% and compared to the base simulation. Sensitivity tests were
10 also performed assuming that the loss of NO_2 on the quartz surface led to HONO formation with the
11 same first order rate as the NO_2 loss, or by including a HONO source in the model, independent of
12 NO_2 , with production rates comparable to experimental observations. Additional sensitivity tests
13 focused on decreasing the constrained species by 5–30% to assess the impact of diluting ambient air in
14 the flow tubes, as well as increasing the temperature of the reference flow tube by 2% to 20% to
15 simulate a heat release by the UV filter. Finally, sensitivity tests were performed to investigate
16 whether reactions of OH with NO_z species that produce O_x could significantly impact the OPR
17 measurements. NO_z species producing NO_2 or NO_3 (NO_2 reservoir) in the model when reacting with
18 OH are HONO, HO_2NO_2 , organic nitrates, HNO_3 , PANs and unsaturated PANs. The NO_2 and NO_3
19 products of the reactions mentioned above were removed from the model for the sensitivity test.

20 **2.4 Description of the field measurements**

21 The OPR instrument was deployed in the field, as part of the Indiana Radical, Reactivity and Ozone
22 Production Intercomparison (IRRONIC) campaign in Bloomington, Indiana, during July 2015. The
23 measurements were taken at the Indiana University Research and Teaching Preserve (IURTP) field
24 laboratory (39.1908N, 86.502W), 2.5 km northeast of the Indiana University Bloomington campus.

25 The site is a mixed deciduous forest containing northern red oaks and big-tooth aspens, which are
26 known to be strong emitters of isoprene and monoterpenes (Isebrands et al., 1999; Funk et al., 2005).
27 A highway (E Matlock Road, State Route 45) is located 1 km southwest, and therefore the site can be



1 impacted by anthropogenic emissions. The OPR flow tubes were setup on a scaffolding to expose
2 them to the sunlight for the entire day. The conversion units and the CAPS monitor were housed
3 inside the laboratory and were connected to the flow tubes using 4-m long heated ¼” PFA lines.

4 This campaign included measurements of OH, HO₂* (HO₂+αRO₂), total peroxy radicals (HO₂+RO₂),
5 total OH reactivity, NO_x, O₃, anthropogenic and biogenic VOCs, radiation and meteorological data.
6 For the measurements presented in this publication, VOCs were measured by an online TD-GC/FID,
7 an online TD-GC/FID-MS (Badol et al., 2004; Roukos et al., 2009), and offline samplers for
8 DiNitroPhenylHydrazine (DNPH) cartridges (Waters Sep-Pak) and Sorbent cartridges (Carbopack
9 B/Carbopack C) by IMT Lille Douai. Measurements of NO (chemiluminescence, Thermo model 42i-
10 TL), NO₂ (cavity attenuated phase shift spectroscopy, Aerodyne Research), and ozone (2B Tech
11 model 202 sensor) were also conducted by the University of Massachusetts. Measurements of J(NO₂)
12 were performed using a scanning actinic flux spectroradiometer (SAFS, METCON) from the
13 University of Houston, while meteorological data, including temperature, relative humidity, wind
14 speed and wind direction were measured with a meteorological station from Montana State
15 University.

16 The OPR measurements were focused on investigating the sensitivity of P(O_x) to NO_x (see section
17 3.3). This was achieved by introducing a certain amount of NO (ppbv range) inside the OPR sampling
18 line for 40 minutes, and then stopping the NO addition for another 40 minutes. This pattern was
19 repeated continuously, keeping the NO level constant for several days. The first 20 minutes of each
20 40-minute measurements were discarded, since they correspond to a transient regime between the
21 disturbed-undisturbed P(O_x) measurements due to the long air-exchange time in the flow tubes (see
22 section 3.1.1). The addition of NO in the OPR sampling line was performed through a 1/8”-OD
23 stainless steel tube using a NO cylinder (3.75 ppmv in N₂) from Indiana Oxygen and a mass flow
24 controller. After the mixing point, a length of 10 m of 1/2”-OD PFA tube was used as the sampling
25 line to ensure a good mixing of NO with the sampled air, leading to a residence time of approximately
26 10 s in the line at a total flow rate of 4 L min⁻¹.



1 **3 Results and discussion**

2 **3.1 Laboratory characterization**

3 **3.1.1 Quantification of the flow tubes residence time**

4 As described in the experimental section, pulses of toluene were injected in the flow tubes to quantify
5 the mean residence time. One of the 5 experiments that were conducted is shown in Figure 2. The
6 pulse shape is asymmetric and exhibits a long tail, indicating that a large range of residence times is
7 observed in the flow tubes. The toluene pulse is treated as a probability distribution of the time
8 variable t , with the average residence time in the flow tubes being the mean of the probability
9 distribution. The latter is calculated as a weighted average of the possible values that the time variable
10 can take. The average residence time from the 5 toluene pulse experiments was 4.52 ± 0.22 min (1σ).
11 The uncertainty reported for the residence time will lead to a 4.9% error (1σ) on the $P(O_x)$
12 measurements.

13 Based on the flow tube volume of 10.8 L and a total flow rate of 2.25 L min^{-1} in each flow tube, a
14 laminar plug flow would lead to a residence time of 4.79 min. The measured residence time is
15 approximately 6% lower than the time calculated for laminar flow conditions, which is barely
16 significant considering the 1σ uncertainty of 4.9% determined from the measurements. However, the
17 asymmetry of the peak indicates that the flow rate at the central axis of the tube is larger, with the first
18 molecules of toluene being sampled after approximately 2 minutes (Fig. 2). These observations are
19 similar to that reported by Cazorla and Brune (2010) for sampling chambers exhibiting a different
20 geometry and operated under different flow conditions. In this study, the authors reported a residence
21 time that was 23% lower than plug flow calculations and a similar asymmetric shape for the pulse.
22 Further work is needed to reduce the skewness of the time distribution.

23 Tests were also performed to quantify the air-exchange time in the flow tubes. These tests were
24 performed by sampling a constant concentration of O_x species with the OPR instrument until a stable
25 O_x signal was measured and by quickly changing the O_x concentration at the inlet. The time needed to
26 reach 95% of a new stable O_x signal was defined as the air-exchange time. The air-exchange time was
27 quantified at approximately 20 minutes, corresponding to a maximum residence time of 1200 s. As



1 mentioned in section 2.1, a $P(O_x)$ value is recorded every 2 minutes. Since the air-exchange time is 20
2 minutes, the 2-minute $P(O_x)$ values are not independent from each other and therefore the OPR
3 instrument cannot detect rapid changes of $P(O_x)$. In order to get independent measurements of $P(O_x)$,
4 the OPR measurements are therefore averaged over 20 minutes.

5 **3.1.2 Quantification of O_x losses in the flow tubes**

6 The principle of the OPR instrument requires that the only difference between the two flow tubes is
7 the suppression of gas-phase photolytic reactions leading to the formation of free radicals in the
8 reference tube. All other characteristics, including flow pattern and potential gas-wall interactions
9 should be the same in the two flow tubes so that they cancel out in the differential O_x measurement.
10 However, if O_x losses were slightly different between the two flow tubes, it could significantly impact
11 the $P(O_x)$ measurements. For example, a 2% difference in O_x losses between the flow tubes would
12 lead to a bias of 27 ppbv h^{-1} on the measurements for an ambient O_x level of 100 ppbv and a residence
13 time of 4.5 min.

14 Figure 3 shows the results of NO_2 and O_3 loss tests for the two flow tubes, performed at different
15 dates during one month of field operation during the IRRONIC campaign and at different relative
16 humidity values. All NO_2 loss tests were performed under dark conditions, i.e. with both flow tubes
17 covered by an opaque cover. Figure 3-(a, c, e) shows that the NO_2 loss is lower than 5% in both flow
18 tubes and is close to 3% on average. When the two flow tubes are operated under the same conditions,
19 the relative loss in the reference tube seems to be higher than the loss in the ambient tube by only 1%
20 at most (Fig. 3-e). For an ambient NO_2 mixing ratio of 30 ppbv, a difference of 1% in NO_2 losses
21 between the flow tubes would lead to a 4 ppbv h^{-1} bias in the $P(O_x)$ measurements.

22 Cazorla and Brune (2010) reported an uncertainty of $\pm 14\%$ for the MOPS instrument due to potential
23 differences in relative humidity between the two sampling chambers, which in turn leads to different
24 NO_2 losses. This was mainly due to a higher temperature in the reference chamber, which is covered
25 by the UV filter. However, the fans used in the OPR instrument to flow ambient air between the UV
26 filter and the flow tube minimize the temperature differences between the two tubes, leading to
27 relative humidity differences lower than 4%, as observed during the field testing. Figure 3-e also



1 shows that a decrease in relative humidity from 65% to 0% only leads to a small decrease of the NO₂
2 loss by 1–2%. A small difference of 4% in relative humidity between the two flow tubes is therefore
3 not expected to lead to additional errors in the P(O_x) measurements. Further analysis of the impact of
4 NO₂ losses on the P(O_x) measurements is discussed in the modeling results section.

5 Ozone loss tests were mainly performed under dark conditions. On 28 July however, O₃ losses were
6 measured with (a) the ambient flow tube exposed to the sunlight and the reference tube covered by the
7 UV filter (orange squares), (b) both flow tubes exposed to the sunlight (orange triangles) and (c) both
8 tubes covered by a dark cover (orange circles). For the first days of the campaign (29 June–8 July), a
9 close inspection of the measurement scatter shown in Figure 3-(b, d) indicates that the relative loss of
10 O₃ is at most close to 5%. However, ozone loss tests performed on 28 July, after one month of
11 operation in the field, reveal an increase of the relative loss up to 13–15%. Additional tests made in
12 the laboratory after the field deployments have shown that this loss can be reduced below 5% if the
13 quartz flow tubes are conditioned with elevated O₃ mixing ratios at high relative humidity for a few
14 days. These results indicate that unsaturated organic species may adsorb on the quartz surface and
15 may react with O₃.

16 Particular attention should be paid to the three different tests performed on 28 July regarding the
17 irradiation conditions. When the losses are quantified under dark conditions (orange circles in Fig. 3-
18 f), the losses are equal between the two flow tubes and close to 13%. However, when the ambient
19 flow tube is irradiated and the reference is covered by the UV filter (orange squares), it can be seen
20 that the relative loss in the ambient tube is higher than in the reference by approximately 3%. Box
21 modeling has shown that the gas-phase photolysis of O₃ in the ambient flow tube could at most
22 account for 0.05% of this additional ozone loss. Therefore, there seems to be a photo-enhanced ozone
23 loss that takes place when the ambient flow tube is irradiated. For an ambient O₃ level of 50 ppbv, this
24 difference in O₃ losses would lead to a negative P(O_x) bias of approximately 20 ppbv h⁻¹. This photo-
25 enhanced loss of ozone is further discussed in the field deployment section (3.3).



1 3.1.3 Heterogeneous HONO production in the flow tubes

2 The formation of HONO in the flow tubes was investigated in the laboratory by sampling humid zero
3 air (25-80% RH) enriched with NO₂ at various mixing ratios (0-100 ppbv) and by measuring HONO
4 mixing ratios in the tubes as described above in section 2.2. Both clean and contaminated (used for
5 more than one month during the IRRONIC campaign) flow tubes were tested to assess the magnitude
6 of HONO production rates and to examine whether there is a dependence on NO₂ mixing ratios,
7 humidity and irradiation. Mixing ratios of HONO up to 250 and 700 pptv were measured under dark
8 conditions for clean and contaminated flow tubes, respectively. Higher mixing ratios of up to 1.5 ppbv
9 were measured under irradiated conditions in the ambient flow tube ($J(\text{NO}_2)=1.4\times 10^{-3} \text{ s}^{-1}$;
10 $J(\text{HONO})=3.1\times 10^{-4} \text{ s}^{-1}$).

11 Dividing the measured mixing ratios of HONO by the residence time in the flow tubes (i.e. 4.5 min),
12 an average production rate can be calculated under dark and irradiated conditions. It is important to
13 note, however, that HONO is also photolyzed at the wavelengths emitted by the lamps (312 nm and
14 365 nm) and production rates calculated under irradiated conditions represent lower bounds. It is
15 estimated that for the $J(\text{HONO})$ value mentioned above and a negligible loss of HONO from
16 OH+HONO, the HONO production rate will be underestimated by less than 8%. The dark HONO
17 production is on the order of 9 ppbv h⁻¹ in both flow tubes, while the total HONO production under
18 irradiated conditions (dark + photo-enhanced) can reach up to 20 ppbv h⁻¹ in the ambient flow tube. In
19 the reference flow tube, the UV light did not impact the formation of HONO, since wavelengths
20 below 400 nm are blocked by the UV filter.

21 The HONO production rate was not observed to depend on NO₂ or humidity and HONO could be
22 even released when no NO₂ was introduced into the contaminated flow tubes. These results strongly
23 suggest that nitro-containing compounds and organic photosensitizers were adsorbed on the walls of
24 the flow tubes and that the HONO production rate depends on contamination levels. Indeed, it was
25 observed that flowing humid zero air in the flow tubes for a few days could reduce the HONO
26 production rate to negligible levels.



1 **3.1.4 Quantification of the conversion efficiency**

2 Based on kinetic considerations for the titration reaction of O₃ by NO, i.e. a rate constant of 1.80×10⁻¹⁴
3 cm³ molecule⁻¹ s⁻¹ at 298K (Atkinson et al., 2004), a reaction time of 23 seconds, and the addition of
4 500 ppbv of NO in the conversion unit, an O₃-to-NO₂ conversion efficiency of 99.5% is expected.
5 These calculations are shown in Figure 4 (black solid line) for different mixing ratios of NO (50–800
6 ppbv) together with laboratory measurements (symbols) made at different O₃ levels. This figure
7 shows that a plateau of almost 100% of conversion is observed at NO mixing ratios higher than 500
8 ppbv. These experimental results are in good agreement with the calculated curve, although the
9 measurements performed at a low O₃ mixing ratio of 3.5 ppbv slightly underpredict the curve for NO
10 mixing ratios lower than 500 ppbv. However, the conversion plateau is reached for all O_x levels and
11 both conversion units (one for each flow tube) for NO mixing ratios higher than 500 ppbv. During the
12 field deployment of the instrument, an NO mixing ratio of 650 ppbv was used to ensure that the
13 difference in conversion efficiency between the two mixing chambers was lower than 0.1% and could
14 be assumed to be 100% for both chambers.

15 In the first version of MOPS (Cazorla and Brune, 2010) the NO₂-to-O₃ conversion was performed by
16 photolyzing NO₂ using a light-emitting diode, achieving a maximum conversion efficiency of 88% at
17 17 ppbv of NO₂. In the most recent version of the instrument (Baier et al., 2015), the conversion
18 efficiency was increased to 88–97% for NO₂ mixing ratios lower than 35 ppbv using a highly-efficient
19 UV lamp that provided ten times more photons than the light-emitting diodes. In the MOPS
20 instrument, however, the conversion efficiency depends on NO₂ levels, as well as on the intensity of
21 the lamp that could drift during a long period of use in the field. In the OPR instrument, the
22 conversion efficiency is stable and does not depend on O₃ mixing ratios. On the other hand, an NO
23 cylinder is required to perform the conversion and possible NO₂ impurities in the cylinder have to be
24 monitored. Indeed, NO₂ impurities coming either from the NO mixture or from NO oxidation in the
25 lines were observed, but were kept at low levels of approximately 6–10 ppbv. Since this impurity is
26 present in both the ambient and reference channel, it does not affect the P(O_x) determination.



1 **3.1.5 Detection limit of the OPR**

2 The detection limit (DL) of the CAPS monitor was quantified by sampling zero air for several hours
3 after several days of conditioning with ambient air. The time resolution was set to 1 s and the zero
4 measurements were averaged over 45 s segments, corresponding to the OPR measurement averaging
5 time. The detection limit (3σ) for a 45 s integration time was quantified at 34 pptv. This detection
6 limit for NO_2 together with a residence time of 4.5 min in the flow tubes should lead to a detection
7 limit of 0.6 ppbv h^{-1} for 2-min $\text{P}(\text{O}_x)$ measurements (1-min measurement from each flow tube).
8 However, nighttime measurements made during the IRRONIC field campaign revealed that the
9 measurement scattering for the complete setup (flow tubes + O_3 -to- NO_2 conversion unit + CAPS) was
10 significantly larger than that expected from the noise of the CAPS monitor. Based on the observed
11 nighttime 1σ variability of 2.1 ppbv h^{-1} , a limit of detection (3σ) of 6.2 ppbv h^{-1} was inferred for the
12 OPR instrument. The scatter in $\text{P}(\text{O}_x)$ measurements does not only depend on the precision of the
13 CAPS monitor, but also depends on how fast each flow tube responds to variations of O_x at the inlet.
14 Indeed, if the time constant for the response is slightly different between the 2 flow tubes, fluctuations
15 of O_x species at the inlet will introduce some scatter in the OPR measurements. In addition, small
16 changes in temperature and humidity may evenly affect O_x losses in each flow tube, leading to
17 additional scatter in the $\text{P}(\text{O}_x)$ measurements.

18 **3.2 Numerical Modeling**

19 As mentioned in the experimental section, several days from different field campaigns were selected
20 to model ambient $\text{P}(\text{O}_x)$, $\text{P}(\text{O}_x)$ in both flow tubes, and the impact of some operating conditions on the
21 OPR measurements. The results from 30 May 2010 of the CalNex field campaign were selected to
22 illustrate the discussion and results from the other days are shown in the supplementary material
23 (Figs. S4, S5, S7-S9). A detailed analysis of the chemistry occurring in each flow tube is discussed
24 below to assess the reliability of OPR measurements.

25 **3.2.1 Radical budget in flow tubes**

26 An analysis of the radical budget was performed in each flow tube to gain insights into the processes
27 driving radical production and loss routes. Figure 5 shows the production and loss rates of OH (upper



1 panel) and peroxy radicals (lower panel) for each flow tube on 30 May 2010 during CalNex. The
2 production and loss rates were calculated taking into account initiation, propagation and termination
3 processes as described below.

4 OH production rates were calculated from photolytic reactions involving closed shell molecules (O_3 ,
5 HONO, H_2O_2 , HNO_3 , HO_2NO_2 and organic peroxides), reactions of O_3 with alkenes, and the
6 propagation of HO_2 by reaction with NO. Loss routes of OH includes propagation reactions to HO_2
7 and RO_2 by reaction with CO and VOCs and termination reactions of OH with NO_2 and other species
8 (NO , PANs, HNO_3 , HONO and HNO_4). For peroxy radicals, production routes include the photolysis
9 of organic species (carbonyls, organic peroxides and organic nitrates), the ozonolysis of alkenes, PAN
10 decomposition, and the propagation of OH. Loss routes were calculated from reactions of peroxy
11 radicals with NO_x , self or cross reactions between peroxy radicals and propagation of HO_2 to OH.

12 Figure 5 clearly shows that the UV filter covering the reference flow tube leads to a decrease of the
13 initiation rates of all radicals by more than a factor of 10 and a decrease of their propagation rates by
14 at least a factor of 30. In the ambient flow tube, photolytic reactions of OVOCs are the most important
15 initiation routes of peroxy radicals, with a contribution of approximately 95%. HONO and O_3
16 photolysis are the most important initiation routes of OH, contributing by approximately 45% each. In
17 the reference flow tube, the primary route of radical initiation is O_3 -alkenes reactions since
18 wavelengths below 400nm are suppressed.

19 The propagation reactions are important in both flow tubes for the production and loss of OH and
20 peroxy radicals. However, the partitioning between initiation and propagation processes is different in
21 the two tubes, which in turn leads to different OH chain lengths. The OH chain length is calculated as
22 the rate of propagation of HO_2 to OH divided by the total initiation of RO_x radicals. As can be seen
23 from Figure 5, the OH chain length is fairly constant at a value of 3 in the ambient flow tube, while in
24 the reference flow tube it quickly decreases to unity for most of the day and to values lower than 1 in
25 the late afternoon. Therefore, in addition to lowering initiation rates of radicals, the UV filter allows to
26 reduce ozone production by lowering the cycling efficiency within the pool of RO_x radicals.



1 A close inspection of the radical termination rates in Figure 5 indicates that the peroxy-NO_x
2 termination reactions are almost suppressed in the reference flow tube. This observation is also
3 supported by Figure S6, which shows time series of the peroxy radicals (HO₂ and RO₂) and NO in
4 each flow tube at a residence time of 4.5 min. Since NO₂ photolysis is almost eliminated in this tube,
5 the O₃-NO_x PSS is shifted towards NO₂ due to the reaction of NO with O₃. As a result, NO mixing
6 ratios in the reference flow tube are at least one order of magnitude lower than in the ambient flow
7 tube. The propagation rate from HO₂+NO is therefore reduced and the OH+NO₂ loss route is
8 enhanced, leading to the shorter OH chain length discussed above. It is also interesting to note that
9 peroxy radical mixing ratios in the reference flow tube are on the same order of magnitude as in the
10 ambient flow tube. This counterintuitive observation is also due to the consumption of NO in the
11 reference flow tube that leads to a longer lifetime for the peroxy radicals, as shown in Figure S6.

12 Calculating P(O_x) from Equations (1-3) results in ozone production rates in the ambient flow tube,
13 $P(O_x)_{amb}$, in good agreement with the modeled $P(O_x)_{atm}$ values, as shown in Figure 6, with a small
14 underestimation of approximately 10% on average. However, significant ozone production rates are
15 also observed in the reference flow tube, which can reach up to 4 ppbv h⁻¹ on this day, while higher
16 values were observed on other days (e.g. 30 ppbv h⁻¹ on 21 March 2006 of the MCMA-2006
17 campaign, Figure S10 in the supplementary material). Ozone production rates in the reference flow
18 tube are about 10–15% of that observed in the ambient flow tube for most of the day. It is important to
19 note, however, that this ozone production is in reality O_x (=O₃+NO₂) production, since NO₂ photolysis
20 is almost suppressed in the reference flow tube. These results indicate that the assumptions initially
21 made on the principle for P(O_x) measurements, i.e that P(O_x) in the ambient flow tube mimics P(O_x)
22 in the atmosphere and P(O_x) in the reference flow tube is not significant, are not completely fulfilled.
23 Based on the modeling results discussed above, the accuracy of the measurements could be
24 significantly impacted by O_x production in the reference flow tube.

25 $P(O_x)_{OPR}$ was calculated from Eq. (6), using an O₃-to-NO₂ conversion efficiency of 100%, and is
26 also shown in Figure 6. As discussed above, $P(O_x)_{OPR}$ underestimates the modeled $P(O_x)_{atm}$,
27 mainly due to significant O_x production in the reference flow tube. The scatter plot shown as insert in



1 this figure indicates that a negative bias of approximately 20% would be observed for $P(O_x)$
2 measurements performed on this day. A negative bias ranging from 15–20% was observed during the
3 other three days that were modeled (Figure S11).

4 As mentioned in the experimental section, concentrations of peroxy radicals obtained as model
5 outputs from the modeling of $P(O_x)_{atm}$ were constrained for the simulations inside the flow tubes,
6 assuming that most of these species are not lost if a short high-flow rate sampling inlet is used.
7 However, simulations were also performed without constraining the peroxy radicals to assess the
8 impact on the simulation results. These simulations have shown that $P(O_x)$ are lower by 10% and 30%
9 in the ambient and reference flow tubes, respectively, when peroxy radicals are not constrained.
10 Overall, the measured ozone production, which is the difference between $P(O_x)$ in the two flow tubes,
11 would only decrease by 2–4%. Therefore, not constraining peroxy radicals in the simulations does not
12 impact the comparison between $P(O_x)_{atm}$ and $P(O_x)_{OPR}$, with $P(O_x)_{OPR}$ underestimating $P(O_x)_{atm}$
13 by 15–20 %.

14 However, the reason for this disagreement depends on whether peroxy radicals are constrained. When
15 peroxy radicals are constrained, the disagreement is mainly caused by O_x production in the reference
16 flow tube. On the opposite, when peroxy radicals are not constrained, this disagreement is due to an
17 underestimation of $P(O_x)_{atm}$ by $P(O_x)_{amb}$. This underestimation is the result of a latency in the first
18 part of the ambient flow tube due to the time needed to reproduce the radicals, which is on the order
19 of 1–2 minutes. It is very likely that only a fraction of the peroxy radicals will be transferred to the
20 flow tubes and a combination of the two issues discussed above will lead to the negative bias of 15–
21 20%.

22 **3.2.2 Sensitivity tests - Assessment of the impact of operating conditions on OPR** 23 **measurements**

24 Figure 7 shows the dependence of $P(O_x)_{OPR}$ on the O_3 -to- NO_2 conversion efficiency, O_3 and NO_2
25 surface-losses, surface-production of HONO, and a dilution of the sampled air. The results are
26 displayed for two different times of the day, characterized by different O_3 and NO_2 mixing ratios,
27 which have been identified as upper (orange squares) and lower (blue squares) limits for the impact



1 on the $P(O_x)$ measurements. In addition, these results are also displayed using daily averaged values
2 (green triangles), which are more representative of the average impact of a particular parameter on
3 $P(O_x)$ measurements. The figures described below are for the CalNex campaign during 30 May 2010.
4 Results from the other days are shown in the supplementary material (Figures S12-S14).

5 Figure 7-a shows that $P(O_x)_{OPR}$ is very sensitive to the O_3 -to- NO_2 conversion efficiency. For
6 instance, a conversion efficiency of 85% would lead to an underestimation of the $P(O_x)$ measurements
7 by 20–60% ($\approx 35\%$ on average), depending on the chemical composition of the air mass. It is
8 interesting to see that the change in $P(O_x)_{OPR}$, expressed as the ratio between $P(O_x)_{OPR}$ at a
9 conversion efficiency lower than 100% and $P(O_x)_{OPR}$ at a conversion efficiency of 100% (base
10 simulation), changes linearly with the conversion efficiency. The slope of the straight line can be used
11 as an indicator to gauge the impact of the conversion efficiency on $P(O_x)$ measurements throughout
12 the day. As can be seen from Equation (6), for the limiting case of $C=0$, the measured $P(O_x)$ is
13 determined by the absolute NO_2 difference between the two flow tubes. The O_3 - NO_x PSS is shifted
14 towards NO_2 in the reference flow tube, due to the lack of NO_2 photolysis, reducing the NO_2
15 difference between the two tubes and lowering the measured $P(O_x)$. These results stress out the need
16 to reach a conversion efficiency better than 98% to keep this artifact below 5%. The OPR instrument
17 described in this study exhibits a conversion efficiency higher than 99.9% and is not impacted by this
18 issue.

19 Relative surface-losses of 3% and 5% have been observed for NO_2 and O_3 , respectively, during the
20 laboratory and field testing (section 3.1.2). Figure 7-b shows that a relative NO_2 loss of 3% in the flow
21 tubes can lead to an overestimation of up to 8% ($\approx 3\%$ on average). On the other hand, Figure 7-c
22 shows that a 5% relative loss of O_3 can lead to an underestimation of up to 30% ($\approx 5\%$ on average).
23 These contrasting effects can be explained as follows; ozone in the reference flow tube is lower than
24 in the ambient flow tube, due to the conjunction of a lower production rate of ozone and a shift of the
25 O_3 - NO_x PSS towards NO_2 . A similar relative loss of ozone in the two flow tubes will therefore lead to
26 a larger absolute loss of O_x species in the ambient flow tube, which in turn will lead to an
27 underestimation of the $P(O_x)$ measurements (Eq. (6)). In contrast, NO_2 is higher in the reference flow



1 tube and a loss of NO_2 will lead to a larger absolute loss of O_x species in the reference flow tube, and
2 as a consequence, to an overestimation of the $\text{P}(\text{O}_x)$ measurements.

3 Figure 7-d shows how an heterogeneous production of HONO can impact the $\text{P}(\text{O}_x)$ measurements. In
4 these simulations, a HONO source was added in the model, with a production rate of 10 ppbv h^{-1} in
5 both flow tubes (dark HONO production) and an additional varying production rate in the ambient
6 flow tube (enhanced HONO production). The x-axis presents the HONO production rate in the
7 ambient flow tube, where 10 ppbv/h corresponds to the dark production only. Moreover, this figure
8 indicates that HONO production rates of 20 ppbv h^{-1} in the ambient flow tube, similar to experimental
9 observations, can lead to an overestimation of the $\text{P}(\text{O}_x)$ measurements by up to 40% ($\approx 27\%$ on
10 average). This overestimation results from HONO photolysis in the ambient tube, which leads to
11 additional OH production, which in turn leads to an enhancement of VOC oxidation rates and ozone
12 production. Additional simulations were also performed assuming that NO_2 molecules lost on the
13 surface were equally converted into HONO in both flow tubes (Fig. 7-f), although it is unlikely that
14 the conversion yield of NO_2 into HONO is 100%. The results indicate that, for a relative NO_2 loss of
15 3%, $\text{P}(\text{O}_x)$ could be overestimated by up to 15% (10% on average). Note that the impact of this
16 HONO formation adds up to the previously discussed overestimation due to the NO_2 loss.

17 Figure 7-e displays how the injection of zero air at the periphery on the PTFE inlets impacts $\text{P}(\text{O}_x)$
18 measurement through a dilution of the sampled air. As can be seen from this figure, a 10% dilution
19 leads to less than 9% underestimation of $\text{P}(\text{O}_x)$.

20 Additional sensitivity tests (not shown) were performed to test the impact of a temperature increase in
21 the reference flow tube due to heat release by the UV filter, as well as reactions of OH with NO_z
22 species that produce NO_2 . A temperature increase of 5% in the reference flow tube (1°C increase at
23 20°C) can lead to an underestimation of up to 5%, while the O_x production from reactions of OH with
24 NO_z species can lead to an overestimation of up to 3%.



1 **3.2.3 Conclusions on potential biases on $P(O_x)_{OPR}$ measurements**

2 From the above discussion, we can conclude that there are two main sources of errors. The first source
3 of errors is due to O_x production in the reference flow tube and the latency for RO_x reformation in the
4 ambient flow tube, the extent of each depending on the fraction of ambient peroxy radicals that is
5 transmitted into the flow tubes. The combination of these two issues can lead to an underestimation of
6 ambient $P(O_x)$ by 15-20% on average for the conditions observed during MCMA-2006 and CalNex-
7 2010. The second main source of errors is caused by a surface-production of HONO in the ambient
8 flow tube. Based on a HONO production rate of 20 ppbv h^{-1} , $P(O_x)$ would be overestimated by
9 approximately 30% on average. Additional sources of errors are due to the 4.9% uncertainty on the
10 flow tube residence time, 5% O_3 and 3% NO_2 surface-losses, the dilution by 10% of the sampled air, a
11 possible temperature increase of 5% in the reference flow tube and O_x production from reactions of
12 OH with NO_z species. Daily averaged values and upper bounds of errors associated with these factors,
13 as derived from all modeled days, are reported in Table 1.

14 Based on the daily average values reported in Table 1, direct sums of the potential negative and
15 positive biases lead to -44% and +40%, respectively. However, the magnitude of each error will
16 depend on atmospheric composition and positive errors will, to some extent, cancel out with negative
17 errors. A quadratic sum of all these potential errors leads a range of $\pm 36\%$. The estimation of these
18 errors are based on ambient conditions observed in two different environments, with different air
19 compositions for 4 different days. It is safe to assume that similar error values would be observed in
20 other urban environments.

21 **3.3 Current limitations for field operation**

22 As mentioned in section 2.4, OPR measurements were performed during the IRRONIC field
23 campaign. Figure 8 displays time series for a subset of measurements performed from 10-14 July
24 2015, including two anthropogenic VOCs (toluene and acetylene), a biogenic VOC (isoprene) and
25 inorganic species (O_3 , NO and NO_2). It is clear from this figure that the measurement site was mainly
26 impacted by biogenic emissions, with isoprene reaching at least 5 ppbv most of the days, while
27 anthropogenic VOCs were low (<500 pptv). In addition, NO_x levels were lower than 3 ppbv on these



1 days, confirming the low impact of anthropogenic emissions. These observations indicate that the
2 photochemistry was mainly driven by the oxidation of biogenic VOCs under low NO_x conditions,
3 similar to that observed in other forested areas (Griffith et al., 2013). Isoprene is very reactive with the
4 hydroxyl radical and the strong diurnal variation of this species led to a large range of OH reactivity
5 (a few s⁻¹ up to 30 s⁻¹, not shown). The conjunction of the latter with low levels of NO_x makes this site
6 of particular interest to study the sensitivity of ozone formation to NO_x by adding NO_x in the OPR
7 instrument as described in the experimental section (section 2.4).

8 Due to the low levels of ambient NO_x, ozone production rates at the site were lower than the OPR
9 detection limit of 6.2 ppbv h⁻¹ (section 3.1.5). Indeed, P(O_x) calculations based on total peroxy radical
10 measurements performed using the Peroxy Radical Chemical Amplifier technique indicated peak
11 ozone production rates of approximately 2 ppbv h⁻¹ (not shown). Ambient measurements performed
12 by the OPR instrument without addition of NO should therefore be scattered around zero within the
13 measurement precision. Figure 8 also displays ΔO_x values (difference in O_x mixing ratios between the
14 two flow tubes) measured by the instrument without the addition of NO (ΔO_x^{zero}, blue diamonds).
15 While ΔO_x^{zero} was scattered around zero during nighttime, it consistently exhibited large negative
16 values during daytime (-1 to -5 ppbv), indicating that O_x mixing ratios in the ambient flow tube were
17 lower than in the reference flow tube.

18 It is interesting to note that ΔO_x^{zero} values are anticorrelated with J(NO₂) (Fig. 8). Covering the
19 ambient flow tube with a similar UV filter than the reference flow tube, i.e. operating the two tubes
20 under similar irradiation, showed that ΔO_x increases towards less negative values and ultimately
21 reaches zero. This behavior indicates that the higher loss rate of O_x species in the ambient flow tube is
22 due to the solar irradiation and points towards a photo-enhanced surface loss of O_x species initiated by
23 photons at wavelengths lower than 400 nm. As ambient NO₂ mixing ratios were much lower than the
24 observed loss of O_x, this photo-enhanced loss involves a loss of ozone. For an ambient O₃ level of 40
25 ppbv, as usually observed during the field measurements, a ΔO_x^{zero} of -3 ppbv corresponds to a 7.5%
26 difference in O₃ losses between the two flow tubes and an ozone loss rate higher by approximately 39
27 ppbv h⁻¹ in the ambient flow tube compared to the reference flow tube. This issue was further



1 investigated in the laboratory. Tests performed using artificial irradiation and mixtures of humid air
2 and ozone confirmed that light-induced processes at wavelength lower than 400 nm lead to a loss of
3 ozone at the surface of the ambient flow tube. It was found that this loss depends on ambient ozone
4 levels, J-values and absolute humidity.

5 This version of the OPR instrument is therefore not suitable to perform ambient $P(O_x)$ measurements
6 since the measured ΔO_x is a combination of ambient ozone production and surface- O_3 losses in the
7 ambient flow tube. For this reason, the OPR measurements were focused on investigating the
8 sensitivity of $P(O_x)$ to NO_x , by recording the relative change in $P(O_x)$ when the chemical composition
9 of ambient air was perturbed by an addition of NO. For these measurements, it is assumed that ΔO_x^{zero}
10 is representative of the instrumental zero and ΔO_x^{zero} measurements are referred as “baseline” in the
11 following. ΔO_x measurements performed with an addition of NO are assumed to deviate from ΔO_x^{zero}
12 due to a change in ozone production in the ambient flow tube, while the surface loss of ozone is
13 assumed to be unchanged. This measurement step is denoted ΔO_x^{NO} . The difference between ΔO_x^{zero}
14 and ΔO_x^{NO} divided by the residence time in the flow tubes therefore provides a quantification of the
15 change in $P(O_x)$, referred as $\Delta P(O_x)$, due to the addition of NO. The validity of the assumption that the
16 O_3 photo-enhanced surface-loss is not disturbed by the addition of NO is discussed below.

17 Investigating the ozone production sensitivity to NO is outside the scope of this paper and we only
18 present measurements performed when 6 ppbv of NO were added in the instrument to illustrate its
19 current performances and limitations. Figure 8 displays time series of ΔO_x^{NO} (orange diamonds) when
20 6 ppbv of NO were added in the flow tubes. When NO is added, there is almost no change in ΔO_x
21 during nighttime. In the absence of sunlight, NO only converts O_3 into NO_2 and the amount of O_x
22 measured by the CAPS monitor does not change. During daytime, ΔO_x^{NO} is higher than ΔO_x^{zero} ,
23 suggesting production of ozone in the ambient flow tube. The difference between ΔO_x^{NO} and ΔO_x^{zero} ,
24 divided by the residence time in the flow tubes, represents the change in ozone production rates and is
25 displayed in the bottom panel of figure 8 as $\Delta P(O_x)$. Changes in ozone production of up to 20 ppbv h⁻¹,
26 well correlated with $J(NO_2)$, are observed for these days. Ozone production being NO_x -limited in



1 this environment, a positive change in $P(O_x)$ is indeed expected when a small amount of NO_x is added
2 to the flow tubes.

3 However, the assumption that the photo-enhanced surface-loss of ozone does not change when NO is
4 added may breakdown for large NO mixing ratios. Indeed, the addition of NO in the flow tubes leads
5 to the conversion of a significant fraction of O_3 into NO_2 , which in turn reduces the absolute loss of
6 O_3 in the ambient flow tube, leading to a shift of the ΔO_x^{zero} baseline to less negative values. $\Delta P(O_x)$
7 values reported in Figure 8 will therefore be the combination of a change in ozone production and a
8 change in the absolute loss of O_3 . If the change in the ozone loss rate is significant compared to the
9 change in the ozone production rate, this could lead to an overestimation of the change in ozone
10 production. An assessment of this measurement bias requires modeling the chemistry in both flow
11 tubes to separate the two contributions, i.e the changes in (i) ozone production and in (ii) ozone loss.
12 While this work is outside the scope of this publication, which focuses on the performances and
13 limitations of the OPR instrument, it is interesting to note that preliminary modeling indicates a bias
14 lower than 5 ppbv h^{-1} when 6 ppbv of NO is added.

15 The field deployment during IRRONIC revealed an additional bias in $P(O_x)$ measurements due to a
16 photo-enhanced loss of ozone at the inner surface of the ambient flow tube and the difficulty to probe
17 changes in $P(O_x)$ when the sampled air mass is perturbed by an addition of NO. Ambient
18 measurements of $P(O_x)$ with the current version of the OPR would necessitates performing frequent
19 zeros of the instrument to track the ozone loss and unfortunately a simple solution to do so was not
20 found. This work shows that the sampling part of the OPR instrument needs to be rethought to remove
21 (or reduce to a negligible level) the photo-enhanced surface-loss of ozone, which is a prerequisite to
22 get an instrument capable of reliable measurements of ozone production rates.

23 **3.4 Comparison to the MOPS instrument and potential improvements for the OPR** 24 **instrument**

25 Previous studies (Cazorla and Brune, 2010; Baier et al., 2015) have shown that measurements of
26 ambient ozone production rates are feasible. Baier et al. (2015) reported that the zero of their MOPS
27 instrument was achieved by removing the UV filter from the reference chamber for a full day to



1 record a diurnal profile of ΔO_x , which was then subtracted from the raw ΔO_x measurements on other
2 days. This zeroing procedure was also tested on the OPR instrument, but led to unrealistically high
3 ambient $P(O_x)$ values of approximately 40 ppbv h^{-1} for the low- NO_x forested environment of
4 IRRONIC. This result also suggests that altering the irradiation conditions of the OPR flow tubes
5 leads to a wrong zero of the instrument. This zeroing technique seems to provide better results for the
6 MOPS instrument and it is possible that the design used for the MOPS sampling chambers or the
7 material used to build them (FEP) make it less sensitive to light-dependent surface reactions.

8 Since the main artifacts on the OPR instrument are caused by heterogeneous surface-reactions in the
9 flow tubes, i.e. HONO production (section 3.2.2) and ozone losses (section 3.2.2 and 3.3), the flow
10 tubes should be redesigned to reduce the impact of physicochemical processes occurring near the
11 quartz surface on the ozone production chemistry occurring at the center of the tubes. For instance,
12 the diameter of the tubes could be increased to reduce the surface-to-volume ratio, and their lengths
13 could be shortened together with an increase of the total flow rate to reduce the contact-time between
14 trace gases and the walls. A shorter residence time would also lead to a shorter air-exchange-time,
15 which in turn would help minimizing the scatter in ΔO_x measurements and would help improve the
16 time resolution necessary to generate independent $P(O_x)$ measurements. However, a shorter residence
17 time would also lead to a lower detection limit and a tradeoff between these 2 parameters will likely
18 have to be made.

19 Another solution worth investigating would be to minimize surface reactions by coating the inner
20 surface of the flow tubes with Teflon or by applying a chemical treatment on the quartz surface,
21 which should help removing reactive sites. The latter has already been applied for laboratory kinetic
22 experiments to clean reactor surfaces. Interestingly, it was reported that this type of treatment can also
23 reduce HONO production on quartz surfaces (Laufs and Kleffmann, 2016).

24 Regarding the deployment of this OPR instruments in the field, a reliable zeroing method would be
25 suitable for both ambient $P(O_x)$ and $P(O_x)$ sensitivity measurements. An interesting solution would be
26 to introduce a radical scavenger in the flow tubes to suppress ozone production, but a suitable
27 compound has yet to be identified.



1 **4 Conclusions**

2 An instrument dedicated to direct measurements of ozone production rates (OPR) was developed and
3 consists of two quartz flow tubes, an O₃-to-NO₂ conversion unit and an Aerodyne CAPS NO₂
4 monitor. This setup, compared to the NO₂-to-O₃ conversion approach previously published in the
5 literature, presents the advantage of a conversion efficiency higher than 99.9%, which is independent
6 of ambient O_x levels. Laboratory and field testing performed to characterize the performance of this
7 instrument showed that dark losses of O₃ and NO₂ inside the flow tubes are lower than 5% and 3%,
8 respectively. However, it was shown that dark ozone losses can increase after a long exposure of the
9 flow tubes in the field and frequent cleaning steps should be performed during nighttime by flowing
10 humid air and O₃ in the tubes to keep the loss below 5%.

11 A modeling exercise taking advantage of measurements from previous urban field campaigns showed
12 that a latency in ozone production in the ambient flow tube and a net ozone production in the
13 reference flow tube can lead to a 18% measurement underestimation of ambient P(O_x) on a daily
14 average for the conditions of the MCMA–2006 and CalNex–2010 field campaigns. However, the
15 magnitude of this underestimation depends on the chemical composition of ambient air and it is
16 recommended to assess this potential bias for future campaigns.

17 Sensitivity tests performed during the modeling exercise highlighted the importance of a high
18 conversion efficiency, since a conversion of 95%, which is only 5% lower than the maximum, could
19 lead to an underestimation of ambient P(O_x) by approximately 20% on a daily average for the two
20 selected field campaigns. A dark surface loss of ozone in the flow tubes would lead to an
21 underestimation of ambient P(O_x), while a NO₂ loss would lead to an overestimation. On a daily
22 average, an underestimation of 10% and an overestimation of 5% were assessed for an O₃ loss of 5%
23 and an NO₂ loss of 2%, respectively. A photo-enhanced production of HONO in the ambient flow
24 tube on the order of 20 ppbv h⁻¹ would also lead to an overestimation of ambient P(O_x) by 27% on a
25 daily average. Overall, a quadratic sum of these potential biases for the conditions of the two urban
26 field campaigns leads to a range of errors of ±37% on a daily average.



1 As shown from the first deployment of the OPR instrument, there is an additional bias due to a photo-
2 enhanced loss of O₃ taking place in the ambient flow tube. This requires improving the sampling
3 design to be able to perform reliable ambient measurements. The first field deployment of the OPR
4 instrument was performed in a low NO_x environment, allowing focusing the study on the sensitivity
5 of ozone production to NO_x. Significant changes in ozone production rates were observed (up to 20
6 ppbv h⁻¹) when 6 ppbv of NO_x were added in the flow tubes, consistent with a NO_x-limited production
7 regime.

8

9 **Acknowledgements**

10 This work was supported by grants from the Regional Council Nord–Pas-de-Calais through the
11 MESFOZAT project, as well as the French National Research Agency (ANR–11–LABX–0005–01)
12 and the European Funds for Regional Economic Development (FEDER) through the CaPPA
13 (Chemical and Physical Properties of the Atmosphere) project. The authors thank the Région Hauts-
14 de-France and the Ministère de l’Enseignement Supérieur et de la Recherche (CPER Climibio) and
15 the European Fund for Regional Economic Development for their financial support. The authors are
16 grateful to Dr. William Bloss and Dr. Leigh Crilley (Birmingham University) for sharing their
17 experience on the OPR technique and for the idea of using quartz flow tubes as sampling chambers
18 for the OPR instrument. The authors are also grateful to Vinod Kumar and Vinayak Sinha (IISER
19 Mohali) who provided support and assistance during the initial development stage of the OPR
20 instrument. Finally, the authors thank the Mechanical Instrument Services at Indiana University for
21 the construction of the flow tube flanges.

22

23

24

25



1 **References**

- 2 Akimoto, H.: Global Air Quality and Pollution, *Science*, 302, 1716-1719, 2003.
- 3 Ashmore, M. R.: Assessing the future global impacts of ozone on vegetation, *Plant, Cell &*
4 *Environment*, 28, 949-964, 2005.
- 5 Atkinson, R., Baulch, D. L., Cox, R. A., Crowley, J. N., Hampson, R. F., Hynes, R. G., Jenkin, M. E.,
6 Rossi, M. J., and Troe, J.: Evaluated kinetic and photochemical data for atmospheric chemistry:
7 Volume I - gas phase reactions of O_x, HO_x, NO_x and SO_x species, *Atmos. Chem. Phys.*, 4, 1461-1738,
8 2004.
- 9 Badol, C., Borbon, A., Locoge, N., Léonardis, T., and Galloo, J.-C.: An automated monitoring system
10 for VOC ozone precursors in ambient air: development, implementation and data analysis, *Analytical*
11 *and Bioanalytical Chemistry*, 378, 1815-1827, 2004.
- 12 Baier, B. C., Brune, W. H., Lefer, B. L., Miller, D. O., and Martins, D. K.: Direct ozone production
13 rate measurements and their use in assessing ozone source and receptor regions for Houston in 2013,
14 *Atmospheric Environment*, 114, 83-91, 2015.
- 15 Bottorff, B., Stevens, P. S., Lew, M., Sigler, P. R., and Dusanter, S.: Measurements of Nitrous Acid
16 (HONO) in an Indiana Forest by Laser Photofragmentation/Laser-induced Fluorescence (LP/LIF),
17 Poster, AGU Fall meeting, American Geophysical Union, 2015.
- 18 Cazorla, M., and Brune, W. H.: Measurement of Ozone Production Sensor, *Atmos. Meas. Tech.*, 3,
19 545-555, 2010.
- 20 Cazorla, M., Brune, W. H., Ren, X., and Lefer, B.: Direct measurement of ozone production rates in
21 Houston in 2009 and comparison with two estimation methods, *Atmos. Chem. Phys.*, 12, 1203-1212,
22 2012.
- 23 Chen, S., Ren, X., Mao, J., Chen, Z., Brune, W. H., Lefer, B., Rappenglück, B., Flynn, J., Olson, J.,
24 and Crawford, J. H.: A comparison of chemical mechanisms based on TRAMP-2006 field data,
25 *Atmospheric Environment*, 44, 4116-4125, 2010.
- 26 Dusanter, S., Vimal, D., Stevens, P. S., Volkamer, R., and Molina, L. T.: Measurements of OH and
27 HO₂ concentrations during the MCMA-2006 field campaign – Part 1: Deployment of the Indiana
28 University laser-induced fluorescence instrument, *Atmos. Chem. Phys.*, 9, 1665-1685, 2009a.
- 29 Dusanter, S., Vimal, D., Stevens, P. S., Volkamer, R., Molina, L. T., Baker, A., Meinardi, S., Blake,
30 D., Sheehy, P., Merten, A., Zhang, R., Zheng, J., Fortner, E. C., Junkermann, W., Dubey, M., Rahn,
31 T., Eichinger, B., Lewandowski, P., Prueger, J., and Holder, H.: Measurements of OH and HO₂
32 concentrations during the MCMA-2006 field campaign – Part 2: Model comparison and radical
33 budget, *Atmos. Chem. Phys.*, 9, 6655-6675, 2009b.



- 1 Fu, J. S., Brill, E. D., Jr., and Ranjithan, S. R.: Conjunctive use of models to design cost-effective
2 ozone control strategies, *Journal of the Air & Waste Management Association* (1995), 56, 800-809,
3 2006.
- 4 Fuchs, H., Holland, F., and Hofzumahaus, A.: Measurement of tropospheric RO₂ and HO₂ radicals by
5 a laser-induced fluorescence instrument, *The Review of scientific instruments*, 79, 084104, 2008.
- 6 Funk, J. L., Jones, C. G., Gray, D. W., Throop, H. L., Hyatt, L. A., and Lerdau, M. T.: Variation in
7 isoprene emission from *Quercus rubra*: Sources, causes, and consequences for estimating fluxes,
8 *Journal of Geophysical Research: Atmospheres*, 110, 2005.
- 9 Geng, F., Tie, X., Guenther, A., Li, G., Cao, J., and Harley, P.: Effect of isoprene emissions from
10 major forests on ozone formation in the city of Shanghai, China, *Atmos. Chem. Phys.*, 11, 10449-
11 10459, 2011.
- 12 Goliff, W. S., Stockwell, W. R., and Lawson, C. V.: The regional atmospheric chemistry mechanism,
13 version 2, *Atmospheric Environment*, 68, 174-185, 2013.
- 14 Green, T. J., Reeves, C. E., Fleming, Z. L., Brough, N., Rickard, A. R., Bandy, B. J., Monks, P. S.,
15 and Penkett, S. A.: An improved dual channel PERCA instrument for atmospheric measurements of
16 peroxy radicals, *Journal of environmental monitoring : JEM*, 8, 530-536, 2006.
- 17 Griffith, S. M., Hansen, R. F., Dusanter, S., Stevens, P. S., Alaghmand, M., Bertman, S. B., Carroll,
18 M. A., Erickson, M., Galloway, M., Grossberg, N., Hottle, J., Hou, J., Jobson, B. T., Kammrath, A.,
19 Keutsch, F. N., Lefer, B. L., Mielke, L. H., O'Brien, A., Shepson, P. B., Thurlow, M., Wallace, W.,
20 Zhang, N., and Zhou, X. L.: OH and HO₂ radical chemistry during PROPHET 2008 and CABINEX
21 2009 - Part 1: Measurements and model comparison, *Atmos. Chem. Phys.*, 13, 5403-5423, 2013.
- 22 Griffith, S. M., Hansen, R. F., Dusanter, S., Michoud, V., Gilman, J. B., Kuster, W. C., Veres, P. R.,
23 Graus, M., de Gouw, J. A., Roberts, J., Young, C., Washenfelder, R., Brown, S. S., Thalman, R.,
24 Waxman, E., Volkamer, R., Tsai, C., Stutz, J., Flynn, J. H., Grossberg, N., Lefer, B., Alvarez, S. L.,
25 Rappenglueck, B., Mielke, L. H., Osthoff, H. D., and Stevens, P. S.: Measurements of hydroxyl and
26 hydroperoxy radicals during CalNex-LA: Model comparisons and radical budgets, *Journal of*
27 *Geophysical Research: Atmospheres*, 121, 4211-4232, 2016.
- 28 Hansen, R. F., Griffith, S. M., Dusanter, S., Rickly, P. S., Stevens, P. S., Bertman, S. B., Carroll, M.
29 A., Erickson, M. H., Flynn, J. H., Grossberg, N., Jobson, B. T., Lefer, B. L., and Wallace, H. W.:
30 Measurements of total hydroxyl radical reactivity during CABINEX 2009 - Part 1: field
31 measurements, *Atmos. Chem. Phys.*, 14, 2923-2937, 2014.



- 1 Hofzumahaus, A., Rohrer, F., Lu, K., Bohn, B., Brauers, T., Chang, C.-C., Fuchs, H., Holland, F.,
2 Kita, K., Kondo, Y., Li, X., Lou, S., Shao, M., Zeng, L., Wahner, A., and Zhang, Y.: Amplified Trace
3 Gas Removal in the Troposphere, *Science*, 324, 1702-1704, 2009.
- 4 Isebrands, J. G., Guenther, A. B., Harley, P., Helmig, D., Klinger, L., Vierling, L., Zimmerman, P.,
5 and Geron, C.: Volatile organic compound emission rates from mixed deciduous and coniferous
6 forests in Northern Wisconsin, USA, *Atmospheric Environment*, 33, 2527-2536, 1999.
- 7 Kanaya, Y., Cao, R., Akimoto, H., Fukuda, M., Komazaki, Y., Yokouchi, Y., Koike, M., Tanimoto,
8 H., Takegawa, N., and Kondo, Y.: Urban photochemistry in central Tokyo: 1. Observed and modeled
9 OH and HO₂ radical concentrations during the winter and summer of 2004, *Journal of Geophysical*
10 *Research: Atmospheres*, 112, 2007.
- 11 Kebabian, P. L., Herndon, S. C., and Freedman, A.: Detection of nitrogen dioxide by cavity attenuated
12 phase shift spectroscopy, *Anal. Chem.*, 77, 724-728, 2005.
- 13 Kebabian, P. L., Wood, E. C., Herndon, S. C., and Freedman, A.: A practical alternative to
14 chemiluminescence-based detection of nitrogen dioxide: cavity attenuated phase shift spectroscopy,
15 *Environ Sci. Technol.*, 42, 6040-6045, 2008.
- 16 Kleinman, L. I., Daum, P. H., Imre, D., Lee, Y. N., Nunnermacker, L. J., Springston, S. R.,
17 Weinstein-Lloyd, J., and Rudolph, J.: Ozone production rate and hydrocarbon reactivity in 5 urban
18 areas: A cause of high ozone concentration in Houston, *Geophysical Research Letters*, 29, 105-101-
19 105-104, 2002.
- 20 Kleinman, L. I.: The dependence of tropospheric ozone production rate on ozone precursors,
21 *Atmospheric Environment*, 39, 575-586, 2005.
- 22 Laufs, S., and Kleffmann, J.: Investigations on HONO formation from photolysis of adsorbed HNO₃
23 on quartz glass surfaces, *Physical Chemistry Chemical Physics*, 18, 9616-9625, 2016.
- 24 Lelieveld, J., Butler, T. M., Crowley, J. N., Dillon, T. J., Fischer, H., Ganzeveld, L., Harder, H.,
25 Lawrence, M. G., Martinez, M., Taraborrelli, D., and Williams, J.: Atmospheric oxidation capacity
26 sustained by a tropical forest, *Nature*, 452, 737-740, 2008.
- 27 Lew, M., Bottorff, B., Sigler, P. R., Stevens, P. S., Sklaveniti, S., Leonardis, T., Locoge, N., Dusanter,
28 S., Kundu, S., Deming, B., Wood, E. C. D., and Gentner, D. R.: HO_x Radical Chemistry in an Indiana
29 Forest Environment: Measurement and Model Comparison, Conference talk, AGU Fall meeting,
30 American Geophysical Union, 2015.
- 31 Liu, Y., and Zhang, J.: Atmospheric Peroxy Radical Measurements Using Dual-Channel Chemical
32 Amplification Cavity Ringdown Spectroscopy, *Analytical chemistry*, 86, 5391-5398, 2014.



- 1 Lu, K. D., Hofzumahaus, A., Holland, F., Bohn, B., Brauers, T., Fuchs, H., Hu, M., Häsel, R., Kita,
2 K., Kondo, Y., Li, X., Lou, S. R., Oebel, A., Shao, M., Zeng, L. M., Wahner, A., Zhu, T., Zhang, Y.
3 H., and Rohrer, F.: Missing OH source in a suburban environment near Beijing: observed and
4 modelled OH and HO₂ concentrations in summer 2006, *Atmos. Chem. Phys.*, 13, 1057-1080, 2013.
- 5 Mao, J., Ren, X., Chen, S., Brune, W. H., Chen, Z., Martinez, M., Harder, H., Lefter, B., Rappenglück,
6 B., Flynn, J., and Leuchner, M.: Atmospheric oxidation capacity in the summer of Houston 2006:
7 Comparison with summer measurements in other metropolitan studies, *Atmospheric Environment*, 44,
8 4107-4115, 2010.
- 9 Mao, J., Ren, X., Zhang, L., Van Duin, D. M., Cohen, R. C., Park, J. H., Goldstein, A. H., Paulot, F.,
10 Beaver, M. R., Crouse, J. D., Wennberg, P. O., DiGangi, J. P., Henry, S. B., Keutsch, F. N., Park, C.,
11 Schade, G. W., Wolfe, G. M., Thornton, J. A., and Brune, W. H.: Insights into hydroxyl
12 measurements and atmospheric oxidation in a California forest, *Atmos. Chem. Phys.*, 12, 8009-8020,
13 2012.
- 14 Monks, P. S.: Gas-phase radical chemistry in the troposphere, *Chemical Society reviews*, 34, 376-395,
15 2005.
- 16 Philipp, H. R., Le Grand, D. G., Cole, H. S., and Liu, Y. S.: The optical properties of a
17 polyetherimide, *Polymer Engineering & Science*, 29, 1574-1578, 1989.
- 18 Prinn, R. G.: The cleansing capacity of the atmosphere, *Annual Review of Environment and*
19 *Resources*, 28, 29-57, doi:10.1146/annurev.energy.28.011503.163425, 2003.
- 20 Pugh, T. A. M., MacKenzie, A. R., Hewitt, C. N., Langford, B., Edwards, P. M., Furneaux, K. L.,
21 Heard, D. E., Hopkins, J. R., Jones, C. E., Karunaharan, A., Lee, J., Mills, G., Misztal, P., Moller, S.,
22 Monks, P. S., and Whalley, L. K.: Simulating atmospheric composition over a South-East Asian
23 tropical rainforest: performance of a chemistry box model, *Atmos. Chem. Phys.*, 10, 279-298, 2010.
- 24 Rao, S. T., Galmarini, S., and Puckett, K.: Air Quality Model Evaluation International Initiative
25 (AQMEII): Advancing the State of the Science in Regional Photochemical Modeling and Its
26 Applications, *Bulletin of the American Meteorological Society*, 92, 23-30,
27 10.1175/2010BAMS3069.1, 2010.
- 28 Ren, X., Harder, H., Martinez, M., Leshner, R. L., Oligier, A., Simpas, J. B., Brune, W. H., Schwab, J.
29 J., Demerjian, K. L., He, Y., Zhou, X., and Gao, H.: OH and HO₂ Chemistry in the urban atmosphere
30 of New York City, *Atmospheric Environment*, 37, 3639-3651, 2003.
- 31 Ren, X., van Duin, D., Cazorla, M., Chen, S., Mao, J., Zhang, L., Brune, W. H., Flynn, J. H.,
32 Grossberg, N., Lefter, B. L., Rappenglück, B., Wong, K. W., Tsai, C., Stutz, J., Dibb, J. E., Thomas
33 Jobson, B., Luke, W. T., and Kelley, P.: Atmospheric oxidation chemistry and ozone production:



- 1 Results from SHARP 2009 in Houston, Texas, *Journal of Geophysical Research: Atmospheres*, 118,
- 2 5770-5780, 2013.

- 3 Rohrer, F., Lu, K., Hofzumahaus, A., Bohn, B., Brauers, T., Chang, C.-C., Fuchs, H., Haseler, R.,
- 4 Holland, F., Hu, M., Kita, K., Kondo, Y., Li, X., Lou, S., Oebel, A., Shao, M., Zeng, L., Zhu, T.,
- 5 Zhang, Y., and Wahner, A.: Maximum efficiency in the hydroxyl-radical-based self-cleansing of the
- 6 troposphere, *Nature Geosci.*, 7, 559-563, [10.1038/ngeo2199](https://doi.org/10.1038/ngeo2199), 2014.

- 7 Roukos, J., Plaisance, H., Leonardis, T., Bates, M., and Locoge, N.: Development and validation of an
- 8 automated monitoring system for oxygenated volatile organic compounds and nitrile compounds in
- 9 ambient air, *J. Chromatogr. A.*, 1216, 8642-8651, 2009.

- 10 Saunders, S. M., Jenkin, M. E., Derwent, R. G., and Pilling, M. J.: Protocol for the development of the
- 11 Master Chemical Mechanism, MCM v3 (Part A): tropospheric degradation of non-aromatic volatile
- 12 organic compounds, *Atmos. Chem. Phys.*, 3, 161-180, 2003.

- 13 Seinfeld, J. H., and Pandis, S. N.: *Atmospheric Chemistry and Physics: From Air Pollution to Climate*
- 14 *Change*, Wiley, 2006.

- 15 Shirley, T. R., Brune, W. H., Ren, X., Mao, J., Leshner, R., Cardenas, B., Volkamer, R., Molina, L. T.,
- 16 Molina, M. J., Lamb, B., Velasco, E., Jobson, T., and Alexander, M.: Atmospheric oxidation in the
- 17 Mexico City Metropolitan Area (MCMA) during April 2003, *Atmos. Chem. Phys.*, 6, 2753-2765,
- 18 2006.

- 19 Sigler, P. R., Bottorff, B., Lew, M., Stevens, P., Léonardis, T., Locoge, N., Dusanter, S., Kundu, S.,
- 20 Deming, B., Wood, E., and Gentner, D.: OH radical reactivity in an Indiana Forest: Measurements
- 21 and model comparisons, Poster, AGU Fall meeting, American Geophysical Union, 2015.

- 22 Stevenson, D. S., Dentener, F. J., Schultz, M. G., Ellingsen, K., van Noije, T. P. C., Wild, O., Zeng,
- 23 G., Amann, M., Atherton, C. S., Bell, N., Bergmann, D. J., Bey, I., Butler, T., Cofala, J., Collins, W.
- 24 J., Derwent, R. G., Doherty, R. M., Drevet, J., Eskes, H. J., Fiore, A. M., Gauss, M., Hauglustaine, D.
- 25 A., Horowitz, L. W., Isaksen, I. S. A., Krol, M. C., Lamarque, J. F., Lawrence, M. G., Montanaro, V.,
- 26 Müller, J. F., Pitari, G., Prather, M. J., Pyle, J. A., Rast, S., Rodriguez, J. M., Sanderson, M. G.,
- 27 Savage, N. H., Shindell, D. T., Strahan, S. E., Sudo, K., and Szopa, S.: Multimodel ensemble
- 28 simulations of present-day and near-future tropospheric ozone, *Journal of Geophysical Research:*
- 29 *Atmospheres*, 111, 2006.

- 30 Stockwell, W. R., Kirchner, F., Kuhn, M., and Seefeld, S.: A new mechanism for regional
- 31 atmospheric chemistry modeling, *Journal of Geophysical Research: Atmospheres*, 102, 25847-25879,
- 32 1997.



- 1 Stockwell, W. R., Lawson, C. V., Saunders, E., and Goliff, W. S.: A Review of Tropospheric
2 Atmospheric Chemistry and Gas-Phase Chemical Mechanisms for Air Quality Modeling,
3 *Atmosphere*, 3, 1, 2011.
- 4 Tan, D., Faloon, I., Simpas, J. B., Brune, W., Shepson, P. B., Couch, T. L., Sumner, A. L., Carroll,
5 M. A., Thornberry, T., Apel, E., Riemer, D., and Stockwell, W.: HO_x budgets in a deciduous forest:
6 Results from the PROPHET summer 1998 campaign, *Journal of Geophysical Research: Atmospheres*,
7 106, 24407-24427, 2001.
- 8 Thornton, J. A., Wooldridge, P. J., Cohen, R. C., Martinez, M., Harder, H., Brune, W. H., Williams,
9 E. J., Roberts, J. M., Fehsenfeld, F. C., Hall, S. R., Shetter, R. E., Wert, B. P., and Fried, A.: Ozone
10 production rates as a function of NO_x abundances and HO_x production rates in the Nashville urban
11 plume, *Journal of Geophysical Research: Atmospheres*, 107, ACH 7-1-ACH 7-17, 2002.
- 12 Whalley, L. K., Edwards, P. M., Furneaux, K. L., Goddard, A., Ingham, T., Evans, M. J., Stone, D.,
13 Hopkins, J. R., Jones, C. E., Karunaharan, A., Lee, J. D., Lewis, A. C., Monks, P. S., Moller, S. J., and
14 Heard, D. E.: Quantifying the magnitude of a missing hydroxyl radical source in a tropical rainforest,
15 *Atmos. Chem. Phys.*, 11, 7223-7233, 2011.
- 16 WHO: Review of evidence on health aspects of air pollution, REVIHAAP Project Technical report,
17 World Health Organization, Regional Office for Europe, 2013.
- 18 Wood, E. C., and Charest, J. R.: Chemical Amplification - Cavity Attenuated Phase Shift
19 Spectroscopy Measurements of Atmospheric Peroxy Radicals, *Analytical chemistry*, 86, 10266-
20 10273, 2014.
- 21



Table 1. Sources of errors on $P(O_x)$ measurement. Upper limits and campaign averages of errors assessed from modeling the selected days of the MCMA-2006 and CalNex-2010 field campaigns (see text). FT: Flow Tube

Sources of errors	Value	Negative bias on $P(O_x)$ average	(upper limit)	Positive bias on $P(O_x)$ average	(upper limit)
Residence time (s)	$271 \pm 13^*$	-4.9%*	(-4.9%*)	+4.9%*	(+4.9%*)
O_3 production in ref. FT & latency in amb. FT		-18%**	(-20%**)	–	–
O_3 loss	5%*	-10%**	(-25%**)	–	–
NO_2 loss	<3%*	–	–	5%**	(+11%**)
HONO production	up to 20 ppbv/h*	–	–	+27%**	(+40%**)
Dilution of sampled air	10%*	-8%**	(-9%**)	–	–
Temperature increase in ref. FT	5%***	-3%**	(-5%**)	–	–
O_x formation from $OH+NO_2$	–	–	–	+3%**	(+3%**)
Conservative sum of biases		-44%	(-64%)	+40%	(+59%)

*from laboratory testing; **from model simulations; ***from estimation

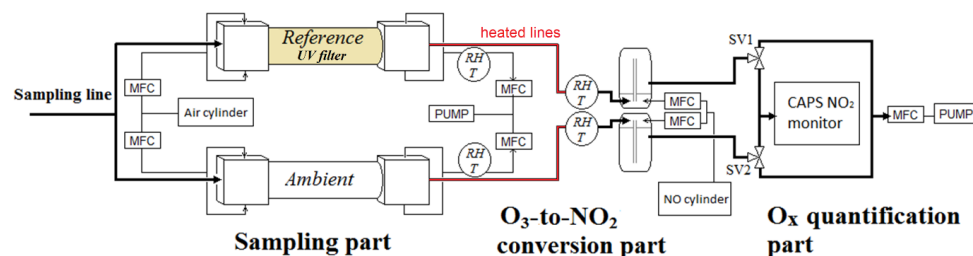


Figure 1. Schematic of the OPR instrument. O_3 converted into NO_2 by reaction with NO . Difference in O_x mixing ratios between the two flow tubes quantified by CAPS. SV: Solenoid Valves. MFC: Mass Flow Controller.

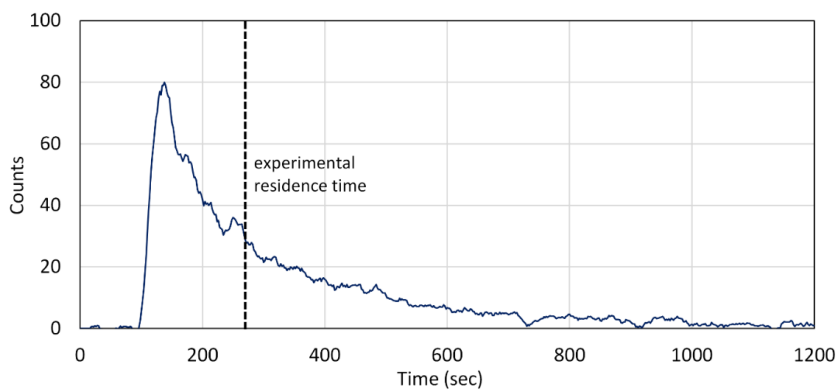


Figure 2. Example of pulse experiments for the quantification of the flow tubes residence time. Pulse of toluene generated at the entrance of the flow tube at $t=0$ s.

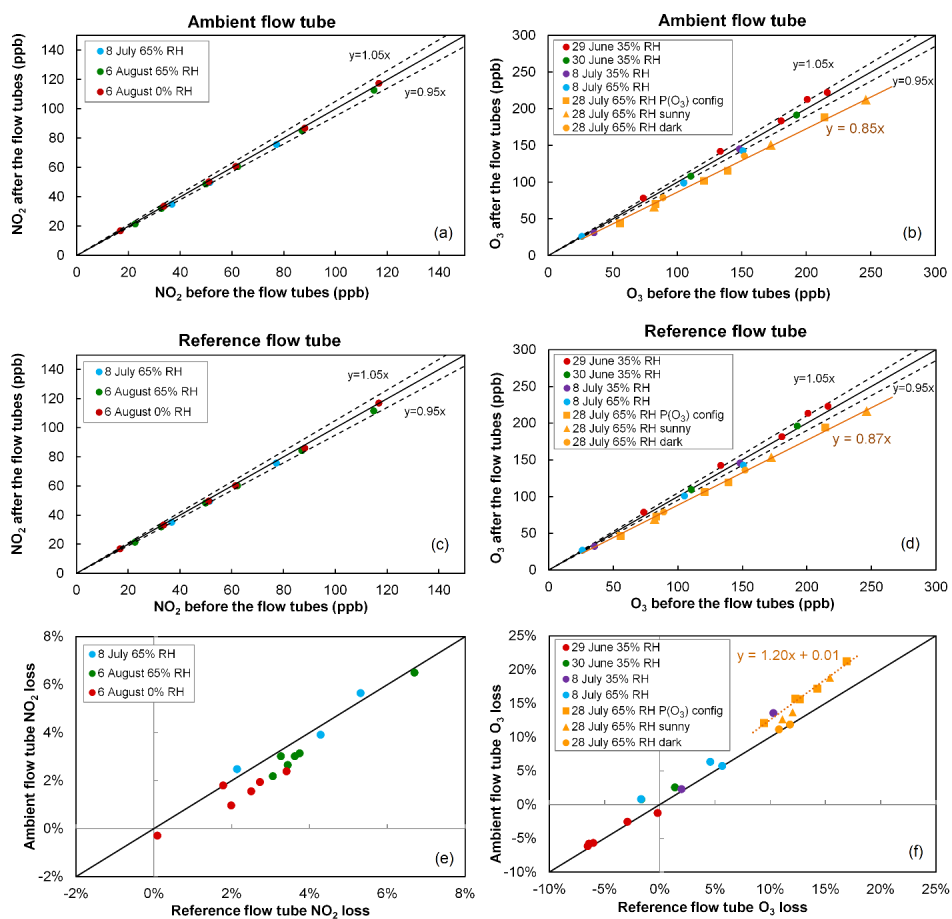


Figure 3. NO₂ and O₃ relative losses measured during the IRRONIC field campaign at different relative humidity values. Losses in the ambient and reference flow tubes are shown in the top and middle panels, respectively. The bottom panel reports the difference in relative losses between the 2 flow tubes. On 28 July O₃ losses were measured under sunny conditions (orange squares: ambient flow irradiated and reference flow tube covered by the UV filter; orange triangles: both flow tubes irradiated), and dark conditions (orange circles: both flow tubes covered by an opaque cover).

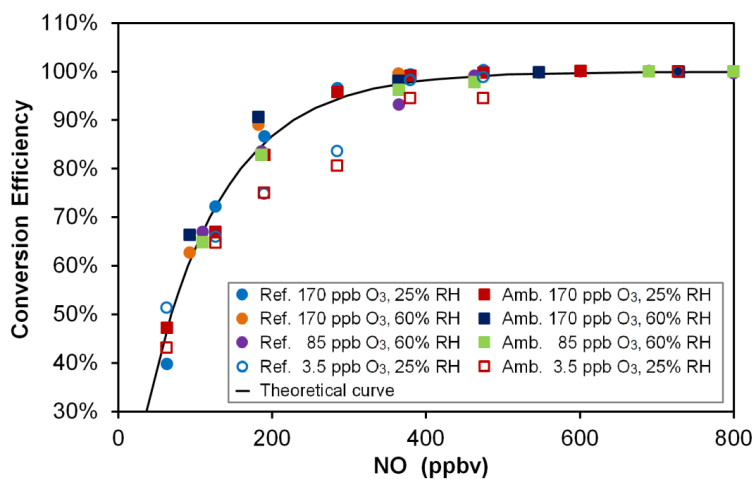


Figure 4. O₃-to-NO₂ conversion efficiency for various NO mixing ratios, O_x levels and relative humidity values. The black curve was calculated from the reaction rate constant between O₃ and NO and a reaction time of 23 s. Open symbols (3.5 ppbv O₃) are hidden behind the plain symbols for NO>500 ppbv. “Ref.” and “Amb.” refer to the conversion units coupled to the reference and ambient flow tubes, respectively.

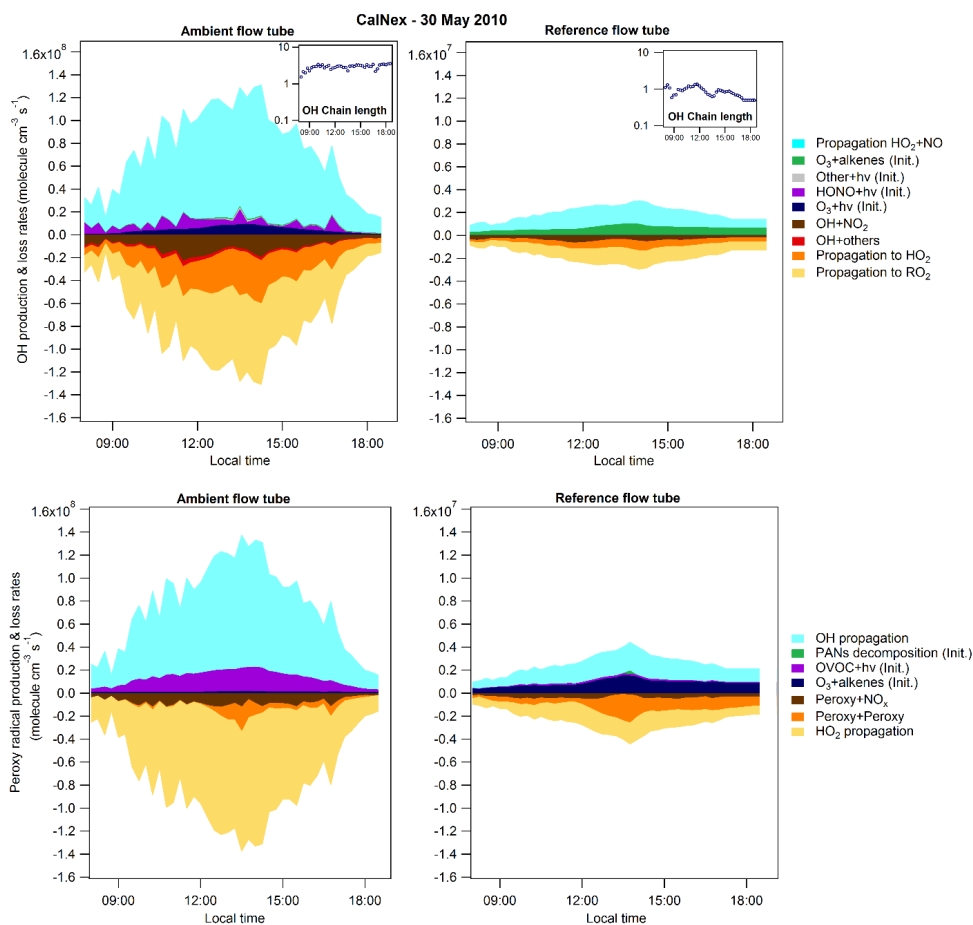


Figure 5. OH (top) and total peroxy (HO_2+RO_2 , bottom) radical budgets for 30 May 2010 of the CalNex–2010 campaign. Radical budgets modeled for the ambient (left) and the reference (right) flow tubes. The OH chain length is also presented in an insert (top) for each flow tube. The note (Init.) in the legend indicates initiation reactions.

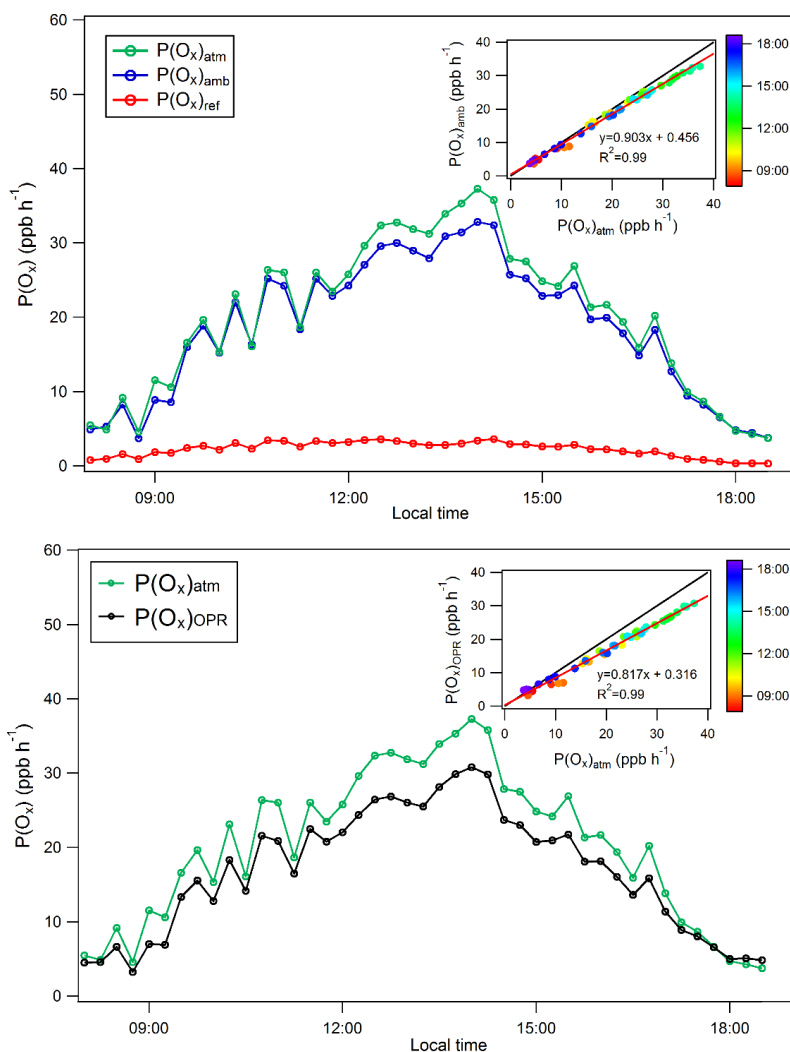


Figure 6. Modeling comparison of $P(\text{O}_x)$ values. Top: ozone production rates modeled for the atmosphere, $P(\text{O}_x)_{\text{atm}}$, the ambient flow tube, $P(\text{O}_x)_{\text{amb}}$, and the reference flow tube, $P(\text{O}_x)_{\text{ref}}$ for 30 May 2010 of the CalNex–2010 campaign. Bottom: comparison of modeled ozone production rates for the OPR, $P(\text{O}_x)_{\text{OPR}}$, and the atmosphere, $P(\text{O}_x)_{\text{atm}}$, for 30 May 2010. Inserts: correlations between $P(\text{O}_x)_{\text{atm}}$ and $P(\text{O}_x)_{\text{amb}}$ (top), and $P(\text{O}_x)_{\text{atm}}$ and $P(\text{O}_x)_{\text{OPR}}$ (bottom), color-coded by the time of day.

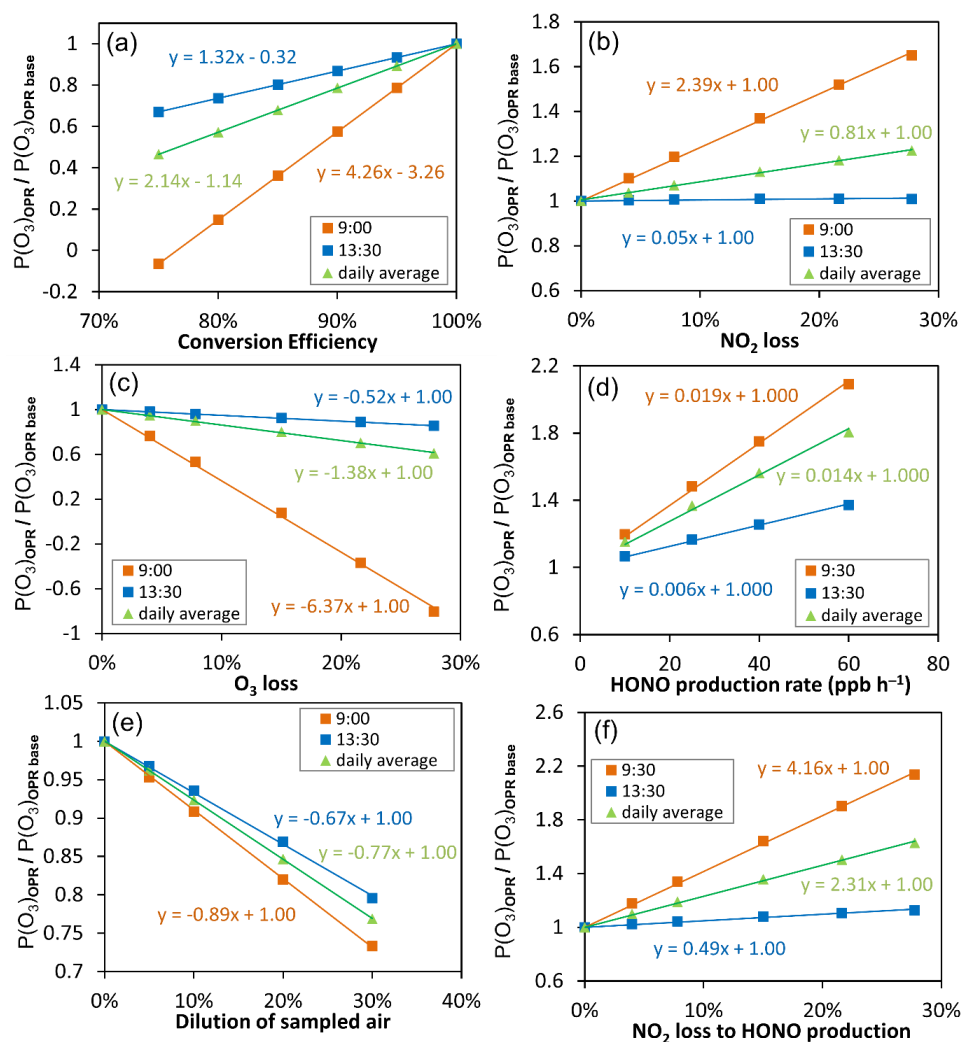


Figure 7. Sensitivity tests performed for 30 May 2010 (CalNex-2010) to assess the impact on the $P(O_x)$ measurements of (a) the O_3 -to- NO_2 conversion efficiency, (b) NO_2 and (c) O_3 dark losses, (d) heterogeneous HONO formation, (e) dilution of ambient air, and (f) NO_2 loss towards HONO production in the flow tubes. The results presented here correspond to the two hours of the day identified as lower (blue squares) and upper (orange squares) limits of the impact on the $P(O_x)$ measurements. The daily average behavior is also shown using green triangles.

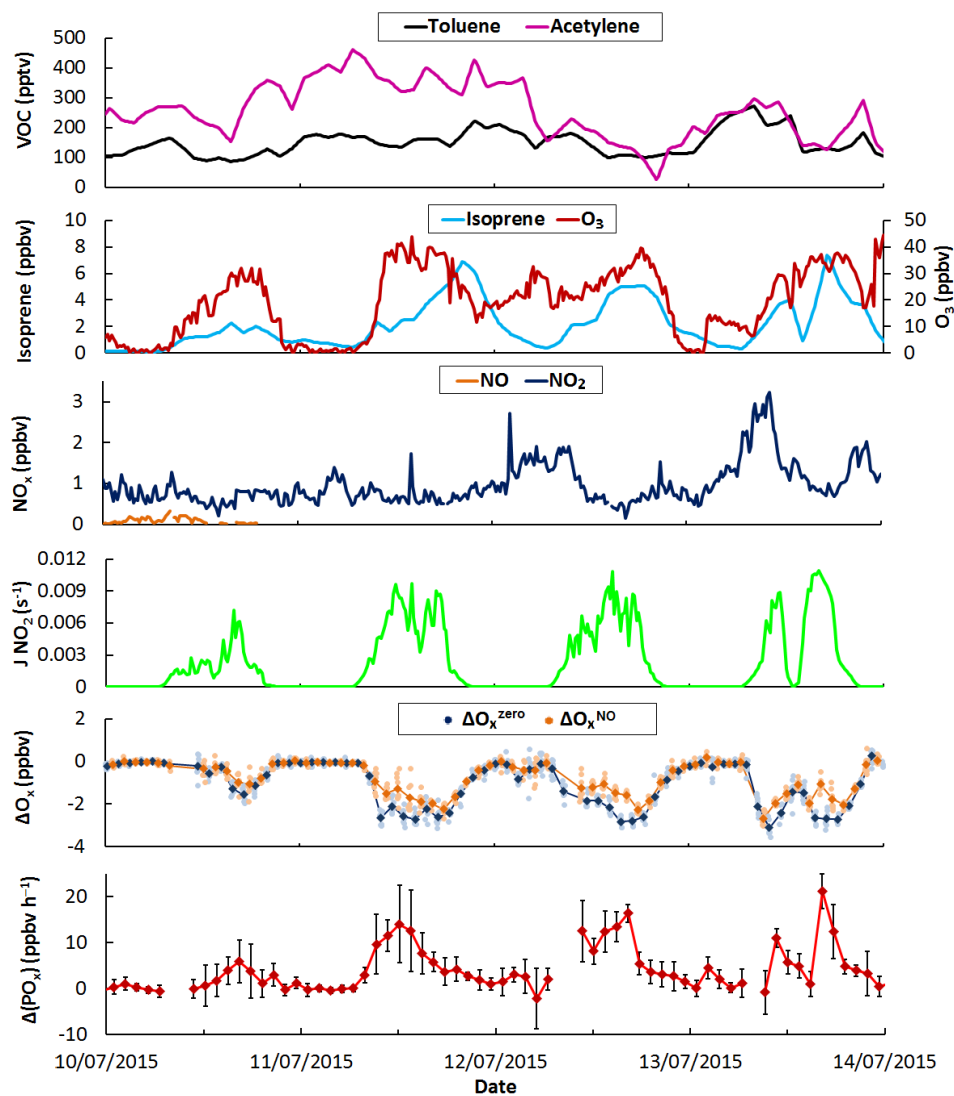


Figure 8. Time series of selected trace gases, $J(\text{NO}_2)$, measured ΔO_x and $\Delta P(\text{O}_x)$ values during four days of the IRRONIC campaign when 6 ppbv of NO was intermittently added in the flow tubes. The light colors on ΔO_x correspond to 2-min measurements while the darker colors are 20-min averaged values. Error bars on $\Delta P(\text{O}_x)$ are 1σ on the averaged 20-min measurements.